Summer 2009

Compensation of Loss and Stimulated Emission of Surface Plasmon Polaritons

Guohua Zhu
Old Dominion University

COMPENSATION OF LOSS AND STIMULATED EMISSION OF SURFACE PLASMON POLARITONS

by
Guohua Zhu
B. A. July 1994, Shanghai Jiaotong University, P. R. China
M. S. March 1999, Shanghai Jiaotong University, P. R. China
M. S. May 2004, Norfolk State University

A Dissertation Submitted to the Faculty of
Old Dominion University in Partial Fulfillment of the
Requirement for the Degree of

DOCTOR OF PHILOSOPHY

ELECTRICAL AND COMPUTER ENGINEERING

OLD DOMINION UNIVERSITY
August 2009

Approved by:

Sacharia Albin (Director)

Mikhail A. Noginov (Co-Director)

Min Song (Member)

Mounir Laroussi (Member)

Carl E. Bonner (Member)

ABSTRACT

COMPENSATION OF LOSS AND STIMULATED EMISSION OF SURFACE PLASMON POLARITONS

Guohua Zhu
Old Dominion University, 2009
Director: Dr. Sacharia Albin (Old Dominion University)
Co-Director: Dr. Mikhail A. Noginov (Norfolk State University)

Surface plasmon polaritons (SPPs) have become in recent years an important research topic because of their interesting physics and exciting potential applications, ranging from sensing and biomedicine to nanoscopic imaging and information technology. However, many applications of surface plasmon polaritons are hindered by one common cause – absorption loss in metal.

Over the years, numerous proposals have been made on how to conquer the plasmon loss. In this dissertation, (1) the known solutions to the loss problem by adding optical gain have been reviewed; (2) the properties of surface plasmon polaritons are studied theoretically, and the solution of the controversy regarding the direction of the k vector of a wave with a strong evanescent component in an active medium has been developed; (3) the propagation of surface plasmon polaritons without gain has been studied experimentally, and it is demonstrated that an addition of highly concentrated rhodamine 6G chloride dye to the PMMA film adjacent to a silver film can cause 30% elongation of the propagation length of surface plasmon polaritons; (4) the propagation of SPPs with optical gain has been studied experimentally and compared to the theoretical predictions: the level of gain achieved in our experiments (≈ 420 cm^{-1} at λ=594 nm) was, in principle, sufficient to compensate the propagation loss of surface plasmon polaritons

in high-quality silver films; and (5) the stimulated emission of surface plasmon polaritons characterized by a distinct threshold in the input-output dependence and narrowing of the emission spectrum has been demonstrated.

The realized compensation of the metallic absorption loss by gain and the observed stimulated emission of surface plasmon polaritons pave the road to a broad range of applications of metamaterials and nanoplasmonic devices.

This dissertation is dedicated to Lei Gu

ACKNOWLEDGMENTS

It is a pleasure to thank the many people who made this dissertation possible. During my PhD studies, I widened the circle of those to whom I am indebted for encouragement, assistance and suggestions.

First of all, I am very grateful to thank my research advisor, Dr. Mikhail A. Noginov. Dr. Noginov, with his knowledge, enthusiasm, smartness and perceptiveness, has provided me the never-ending guidance throughout my years of study since 2002, from my Master's study to the current PhD study.

I would like to acknowledge my appreciation to my principal advisor, Dr. Sacharia Albin, for the inspiration and the encouragement throughout my studies at Old Dominion Univeristy. The assistance of Dr. Carl Bonner, Dr. Min Song, and Dr. Mounir Laroussi in serving on my committee and in reviewing this dissertation is very much appreciated.

Special thanks should also go to my colleagues, Dr. Natalia Noginova, Dr. Suely M. Black, Dr. Vladimir I. Gavrilenko, Dr. Yuri Barnakov, Ms. Shirleigh F. Wood, Ms. Jennifer West, Mr. M. Mayy, and Mr. J. Kitur, who provided wonderful assistance in my research.

The past few years have been the most difficult time of my life. I would like to thank my friends, Sheng Gao and Bin Zhu, Kai Zhang and Wei Feng, Gene Hou and May Hou, Heng Li and Jindong Zhao and many other friends. Without their help, I would never have gotten through the miserable days in my past.

I would like to thank all my family: father, Taizhi Zhu; mother, Yueying Li; sisters Yanhua Zhu & Wanhua Zhu, and brother Tiantian Zhu; back home in China for their love, encouragement and support.

I owe everything in my life to Lei Gu. This doctorate is a testament to everything that I have learned and obtained from her and is my most cherished gift to her as well. I also dedicate this dissertation to my dear daughter, Hanna Zhu.

TABLE OF CONTENTS

Page

Chapter Page

LIST OF FIGURES

Figure Page

Figure Page

Figure Page

Figure Page

Chapter 1
INTRODUCTION

The British Museum has a famous Lycurgus Cup (4th Century A.D.), which changes its color depending on the illumination, Figure 1.1. When viewed in reflected light, for example in daylight, it appears green. However, when a light is shone into the cup and transmitted through the glass, it appears red. Nowadays, it is known that the coloration of the Lycurgus Cup is determined by the frequency of *surface plasmon* resonance in metallic nanoparticles embedded into the glass.

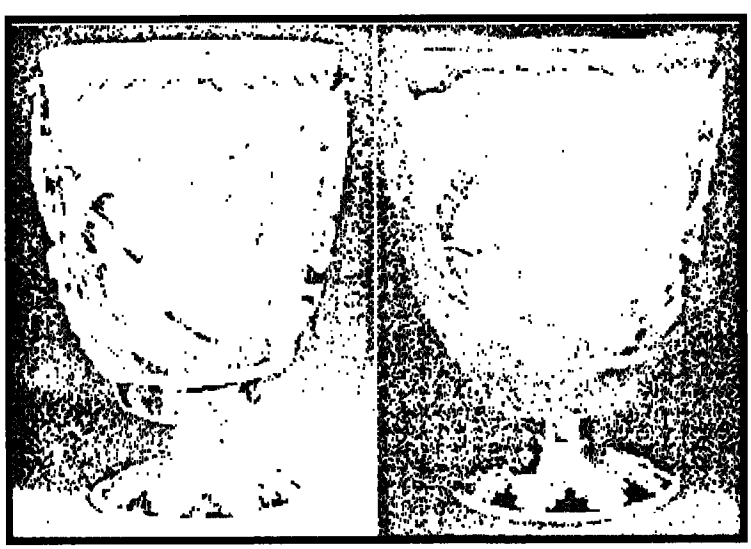

Figure 1.1 Lycurgus Cup (4^{th} Century A.D.) at different illuminations

The format of this dissertation follows the style requirement of *Optics Express, OSA*

1.1 The Idea of Surface Plasmon

In 1957, Ritchie predicted the existence of self-sustained collective excitations at the metal surface by investigating the energy losses of fast electrons passing through thin metal films [1]. Two years later, Powell and Swan experimentally demonstrated the existence of these collective excitations [2, 3] by studying the electron energy losses of aluminum and magnesium, respectively. In 1960, Stem and Ferrell termed such oscillations surface plasmons (SPs) [4].

There are two categories of SPs, depending on the geometrical shape of the interface supporting SPs. One is called localized surface plasmon, which is the oscillation of free electrons in a metallic particle (driven by an external electromagnetic wave), whose resonance frequency is the plasma frequency adjusted by the size and, mainly, the shape of the particle. The famous Lycurgus Cup gives a perfect example for localized surface plasmons. Another one is called surface plasmon polaritons (SPPs), which is a phenomenon relevant to localized SPs. SPP is a surface electromagnetic wave propagating along the interface between two media possessing permittivities with opposite signs, such as metal and dielectric interface.

1.2 The Application of Surface Plasmons

Nanoplasmonics devices have many current and prospective applications, which include but are not limited to surface enhanced near-field microscopy [5], imaging with sub-diffraction resolution [6-10], optical cloaking [11, 12] and nanolasers [13-15].

Localized SPs have been found on rough surfaces [16-18], in engineered nanostructures [19-23], as well as in clusters and aggregates of nanoparticles [24-26]. In

the spots where local fields are concentrated, both linear and nonlinear optical responses of molecules and atoms are gigantically enhanced, thus, dramatically enhancing the Raman signal. This leads to a number of important applications, the most matured of which is the Surface Enhanced Raman Spectroscopy (SERS) [17]. SERS can detect not only the presence of a bimolecular analyte, but also provide a great deal of information on exactly what specific molecules are being detected, which is of particular interest for molecule sensing and bio-applications. A very high sensitivity of SERS enables observation of Raman scattering from a single molecule attached to a metal colloidal particle [27-28].

Brus et al. [29] proposed to use gigantic localized fields to influence the photochemistry of reactions. Later this phenomenon was studied in application to photocells, detectors, and other processes including vision [30]. The enhancement of the response of a p-n junction by localized SPs has been studied recently [31]. A strong field enhancement in the vicinity of a metallic tip enables linear and nonlinear near field scanning microscopy, spectroscopy, and photomodification with nanoscale resolution [32-34]. An extraordinary high transmission of light through periodic arrays of subwavelength holes in metallic films has been explained in terms of resonant excitation of SPs in reference [35]. An enhancement of surface magneto-optical interaction by SPs has been discussed in reference [36].

Negative-index materials (NIMs) have a negative refractive index, so that the phase velocity is directed against the flow of energy. There are no known naturally occurring NIMs in the optical range. However, engineered materials based on nanoplasmonics inclusions, termed as metamaterials, have a negative index of refraction. Metamaterials

can open new avenues to achieving unprecedented physical properties and functionality unattainable with naturally existing materials. NIM was first described by Veselago in his seminal paper [37]. Optical NIMs (ONIMs) promise to create entirely new prospects for controlling and manipulating light, optical sensing, nanoscale imaging and photolithography.

Proof-of-principle experiments [38, 39] have shown that metamaterials can act as NIMs at microwave wavelengths. NIMs drew a large amount of attention after Pendry predicted that a NIM can act as a superlens, allowing an imaging resolution that is limited not by the wavelength but rather by material quality [6]. The near-field version of the superlens has recently been reported by the Zhang and Blaikie groups [40, 41].

While negative permittivity $\varepsilon'<0$ ($\varepsilon= \varepsilon'+ \varepsilon''j$) in the optical range is easy to attain for metals, there is no magnetic response for naturally occurring materials at such high frequencies. Recent experiments showed that magnetic response and negative permeability $\mu'<0$ ($\mu= \mu'+ \mu''j$) can be accomplished at terahertz frequencies [42-44]. These studies showed the feasibility of NIMs because a magnetic response is a precursor for negative refraction. The metamaterial with a negative refractive index at 1.5 μm, based on paired metal nanorods embedded in a dielectric, was designed [45-47] and experimentally demonstrated by the Shalaev group [48-50]. More recently, the results of a sample that displays NIM behavior for red light at a wavelength of 710 nm with index refraction ~ -0.5 has been realized [51]. Additionally, another sample that shows a negative value of ε' and μ' at 725 nm have been observed by the Shalaev group as well [51].

1.3 The Approaches to Conquer the Loss

Most existing and potential future applications of nanoplasmonics suffer from damping caused by metal absorption and radiation losses. Over the years, several proposals have been made on how to conquer the plasmon loss. Thus, in 1989, Sudarkin and Demkovich suggested increasing the propagation length of SPP by creating the population inversion in the dielectric medium adjacent to the metallic film [52]. The proposed experimental test was based on the observation of increased reflectivity of a metallic film in the frustrated total internal reflection setup.

The authors of reference [52] also briefly discussed the possibility of creating an SP- based laser. This work was preceded by the observation of super-luminescence and light generation by a dye solution under the condition of internal reflection [53] and the study of gain-enhanced total internal reflection in the presence of metallic film through the mediation of SPPs on the metal surface [54].

The ideas above have been further developed in more recent years. For example, gain-assisted propagation of SPPs in planar metal waveguides of different geometries has been studied in reference [55]. SPPs at the interface between metal and a dielectric with strong optical gain have been analyzed theoretically by Avrutsky [56]. In particular, it has been shown that the proper choice of optical indices of the metal and dielectric can result in an infinitely large effective refractive index of surface waves. Such resonant plasmons have extremely low group velocity and are localized in a very close vicinity to the interface. The amplification of SPPs at the interface between silver film and dielectric medium with optical gain (laser dye) has been recently demonstrated by Seidel et al. [57]. The observation was done in an experimental setup similar to that proposed in reference

[52], and the experimentally observed change in the metal reflection was as small as 0.001% to 0.01%.

In a similar way, Lawandy has predicted the localized SP resonance in metallic nanospheres to exhibit a singularity when the surrounding dielectric medium has a critical value of optical gain [58]. For the case of a metallic spherical particle of radius $R_{sp}<<\lambda$, and a complex relative dielectric constant $\varepsilon_m(\omega)$, surrounded by an infinite medium with a complex relative dielectric constant $\varepsilon_d(\omega)$, the field is given by [59],

$$E \propto E_0 \frac{1}{2\varepsilon_d(\omega)+\varepsilon_m(\omega)} \tag{1.1}$$

where ω and E_0 are the frequency and amplitude of the linearly polarized incoming plane wave. For simple metals, $\varepsilon_m(\omega)$ can be approximated by the well-accepted Drude model given by [59]

$$\varepsilon_m(\omega) = 1-\omega_p^2\left(\frac{1}{\omega^2 - j\omega\gamma}\right) = 1-\frac{\omega_p^2}{\omega^2}\left(\frac{1}{1+\omega^2\gamma^2}\right)+j\frac{\omega_p^2}{\omega^2}\left(\frac{\frac{\gamma}{\omega}}{1+\omega^2\gamma^2}\right) \tag{1.2}$$

where ω_p is the plasma frequency of the metal and γ is the electron momentum dephasing rate, which is typically two orders of magnitude smaller than ω_p at the room temperature. The complex permittivity of external dielectric medium can be expressed as

$$\varepsilon_d(\omega) = \varepsilon'_d + j\varepsilon''_d \tag{1.3}$$

where ε'_d is the real part and ε''_d is the imaginary part of the dielectric constant.

The singularity, resulting from canceling both real and imaginary terms in the denominator of Eqn. (1.1), can be evidenced by an increase of the Rayleigh scattering within the plasmon band and lead to low threshold random laser action, light localization effects, and enhancement of the surface enhanced Raman scattering [58].

Experimentally, such an idea has been realized in Ref. [60]. Noginov, Zhu, et al. showed the six-fold increase of the Rayleigh scattering has been observed in the dye–Ag aggregate mixture by introducing the gain in the system [60], Figure 1.2, in which a pump–probe Rayleigh scattering experiment was performed. The mixture of Rhodamine-6G (R6G) and Ag aggregate were pumped with a frequency-doubled Q-switched Nd:YAG laser (λ_{pump} =532 nm). A fraction of the pumping beam was split off and used to pump a simple laser consisting of the cuvette with the R6G dye placed between two mirrors, Fig. 1.2 (upper inset). The emission line of the R6G laser (~ 558 nm) corresponded to the maximum of the gain spectrum of the R6G dye in the mixtures studied. The beam of the R6G laser, which was used as a probe in the Rayleigh scattering, was aligned with the pumping beam in the beam splitter and sent to the sample through a small pinhole. The pump and probe beams were collinear. The scattered probe light, along with the scattered pumping light and the spontaneous emission of dye, was collected by an optical fiber that was placed within several millimeters from the cuvette. To separate the scattered probe light, a monochromator was used and recorded the emission spectrum between 540 and 650 nm. The scattered probe light was seen in the spectrum as a relatively narrow (~5 nm) line on the top of a much broader spontaneous emission band, Figure 1.2 (lower inset). Thus it could be easily separated from the spontaneous emission.

Experimentally, the energy of the probe light was kept constant, and the intensity of the scattered probe light as the function of the varied pumping light energy was measured. The six-fold increase of the Rayleigh scattering observed in the dye–Ag aggregate mixture with the increase of the pumping energy (Figure 1.2) is the clear experimental

demonstration of the compensation of the loss in the metal and the enhancement of the quality factor of the SP resonance by optical gain in the surrounding dielectric [60].

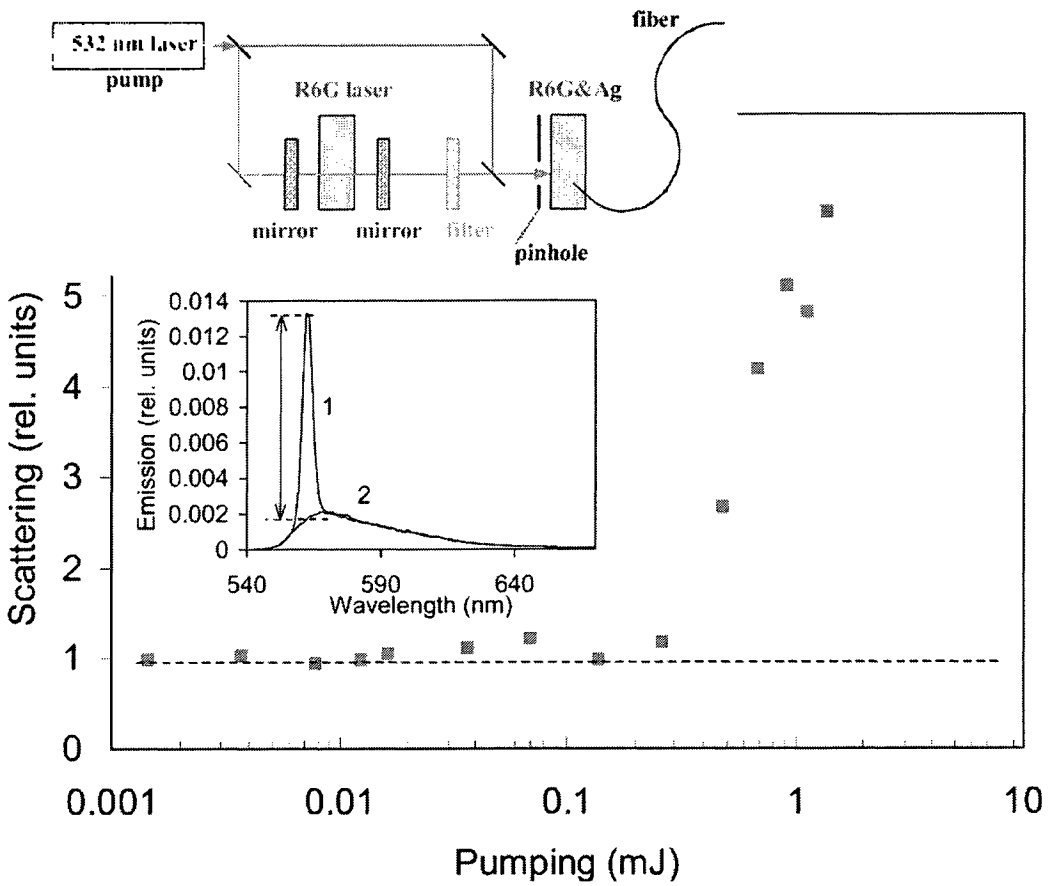

Figure 1.2 Intensity of the Rayleigh scattering as the function of the pumping energy, R6G, $2.1x10^{-5}$ M; Ag aggregate, $8.7x10^{13}$ cm^{-3}. Upper inset: Pump–probe experimental setup for the Rayleigh scattering measurements. Lower inset: 1, spectrum of scattered light and spontaneous emission; 2, spectrum of spontaneous emission only. The difference between the two spectra indicated by the arrow is plotted in the main frame. [60].

In Ref. [61], where a three-component system consisting of (i) metallic nanoparticle, (ii) shell of molecules with optical gain adsorbed onto the metallic nanoparticle, and (iii) surrounding dielectric (solvent) has been studied theoretically. In particular, it has been

shown that depending on the thickness of the layer of an amplifying shell, the absorption of the complex can increase or decrease with the increase of the gain in the dye shell [61].

A seemingly similar phenomenon has been described in an earlier publication [62] using a completely different set of arguments. Thus, Bergman and Stockman [62] have proposed a new way to excite localized fields in nanosystems using surface plasmon amplification by stimulated emission of radiation (SPASER). SPASER radiation consists of SPs (bosons), which undergo stimulated emission, but, in contrast to photons, can be localized on the nanoscale. SPASER consists of an active medium with population inversion that transfers its excitation energy to a resonant SP resonator, which plays a role analogous to the laser cavity [62, 63].

1.4 The Organization of the Dissertation

Chapter 1 gives an introduction to the surface plasmon and surface plasmon polaritons. The current and potential applications of surface plamon are discussed. The methods to conquer the loss of the propagation of surface plasmon are presented.

Chapter 2 presents the theory of surface plasmon polaritons. The wave function of surface plasmon polaritons is derived and the methods to excite the surface plasmon polaritons are discussed as well. The modeling to surface plasmon polaritons is proposed and numerical simulated results are presented.

From Chapters 3 to 5, the experimental results of propagation of surface plasmon polaritons are described, which includes the propagation of surface plasmon polaritons without and with gain, and the stimulated emission of surface plasmon polartions.

Chapter 6 summarizes the dissertation.

Chapter 2

MODELING OF SURFACE PLASMON POLARITONS

The properties of surface plasmon polaritons are studied in this Chapter. The attenuated total reflection is proposed to model the propagation of surface plasmon polaritons. The numerical results are presented, and in particular, the controversy regarding the direction of the wave vector of a wave with a strong evanescent component in an active medium is solved.

2.1 The Properties of Surface Plasmon Polaritons

In order to model the surface plasmon modes, a plane wave is assumed to propagate from one material to another, Figure 2.1. The dielectric constants of two media are ε_1 and ε_2, respectively.

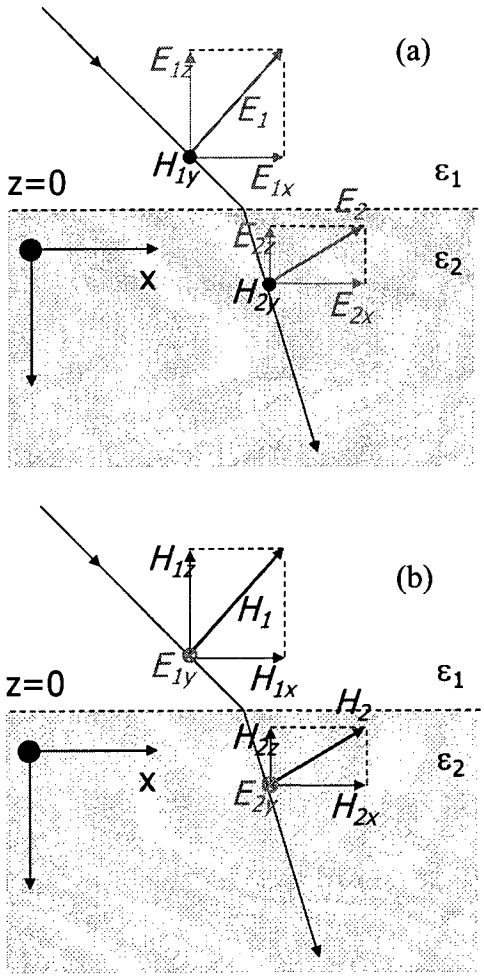

Figure 2.1 p-polarized wave (a) and s-polarized wave (b) propagate from one material to another

If the incident wave is p-polarized, Figure 2.1(a), whose electric field, E_1, is parallel to the plane of incidence, the boundary conditions at the interface of two materials give,

$$E_{1x} = E_{2x}, \tag{2.1}$$

$$D_{1z} = D_{2z}, \tag{2.2}$$

where E_{1x} and E_{2x} are transverse components of E_1 and E_2 respectively, and D_{1z} and D_{2z} are normal components of electric displacement field D_1 and D_2, respectively, which are given by

$$D_{iz} = \varepsilon_o E_{iz} + P_{iz}, i = 1,2, \tag{2.3}$$

where P_{iz} is the z component of the polarization density of the material.

Combining Eqns. (2.2) and (2.3) , one obtains

$$\varepsilon_o E_{1z} + P_{1z} = \varepsilon_o E_{2z} + P_{2z}. \tag{2.4}$$

The Eqn. (2.4) shows polarization charges are created at the interface between two materials. If one of the materials is metal, the electrons will respond to this polarization, giving rise to surface plasmon modes.

If the incident wave is s-polarized, Figure 2.1(b), whose electric field, E_1, is perpendicular to the plane of incidence, the boundary conditions at the interface of two materials only give,

$$E_{1y} = E_{2y}, \tag{2.5}$$

where E_{1y} and E_{2y} are transverse components of E_1 and E_2, respectively. In such case, no polarization charges are created, and no surface plasmon modes are excited.

Let's assume that a p-polarized wave is propagating from the dielectric medium to the metallic medium, as shown in Figure 2.2. The electric and magnetic fields in these two media are given by [64]

$$E_1 = (E_{1x}, 0, E_{1z}) e^{j(k_{1x}x - \omega t)} e^{jk_{1z}z}, \tag{2.6}$$

$$H_1 = (0, H_{1y}, 0) e^{j(k_{1x}x - \omega t)} e^{jk_{1z}z}, \tag{2.7}$$

and

$$E_2 = (E_{2x}, 0, E_{2z}) e^{j(k_{2x}x - \omega t)} e^{jk_{2z}z} \quad , \tag{2.8}$$

$$H_2 = (0, H_{2y}, 0) e^{j(k_{2x}x - \omega t)} e^{jk_{2z}z}, \tag{2.9}$$

where k_{ix} is the component of the wave vector (i =1, 2), which is parallel to the x direction.

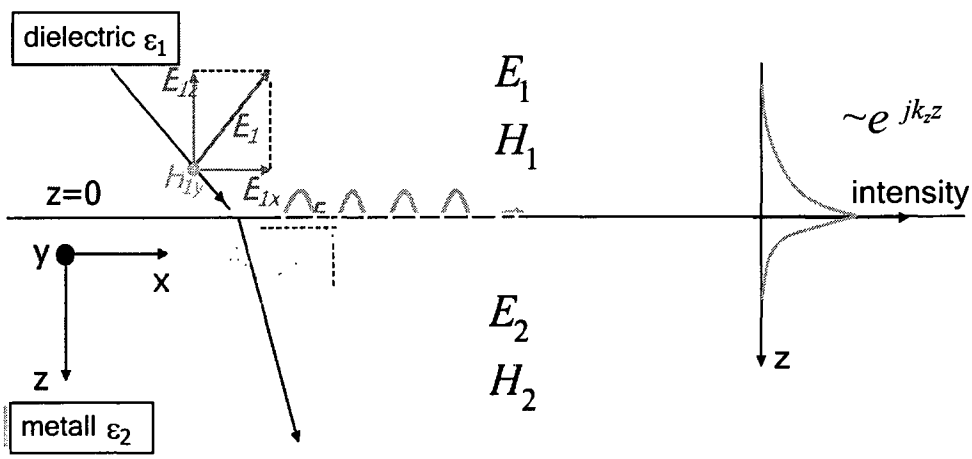

Figure 2.2 p-polarized wave propagates from dielectric medium to metallic medium

These fields have to fulfill the Maxwell's equations:

$$\nabla \times H_i = \varepsilon_i \frac{1}{c} \frac{\partial E_i}{\partial t}, \tag{2.10}$$

$$\nabla \times E_i = -\frac{1}{c} \frac{\partial H_i}{\partial t}, \tag{2.11}$$

$$\nabla \bullet E_i = 0, \tag{2.12}$$

$$\nabla \bullet H_i = 0, \tag{2.13}$$

together with the boundary relations

$$E_{1x} = E_{2x}, \tag{2.14}$$

$$H_{1y} = H_{2y}, \tag{2.15}$$

$$\varepsilon_1 E_{z1} = \varepsilon_2 E_{z2}, \tag{2.16}$$

where c is speed of light.

At z =0, by following the continuity of E and H, one, together with Eqns. (2.14) and (2.15), has

$$k_{x1} = k_{x2} = k_x. \tag{2.17}$$

Eqn. (2.10) gives:

$$\frac{\partial H_{yi}}{\partial z} = -\frac{\omega}{c}\varepsilon_i E_{xi}, i = 1,2 \text{ .or}$$

$$k_{zi} H_{yi} = \frac{\omega}{c}\varepsilon_i E_{xi}, i = 1,2 \tag{2.18}$$

Eqn. (2.18) together with Eqns (2.14) and (2.15) yield:

$$H_{y1} - H_{y2} = 0, \tag{2.19}$$

$$\frac{k_{z1}}{\varepsilon_1} H_{y1} + \frac{k_{z2}}{\varepsilon_2} H_{y2} = 0. \tag{2.20}$$

To obtain a solution for Eqns. (2.19) and (2.20), one has

$$\frac{k_{z1}}{\varepsilon_1} + \frac{k_{z2}}{\varepsilon_2} = 0. \tag{2.21}$$

Further, one gets from Eqns. (2.10), (2.11) and (2.18),

$$\varepsilon_i \left(\frac{\omega}{c}\right)^2 = k_x^2 + k_{zi}^2, i = 1,2 \tag{2.22}$$

Combining Eqns. (2.21) and (2.22), one obtains

$$k_x = \frac{\omega}{c}\left(\frac{\varepsilon_1\varepsilon_2}{\varepsilon_1+\varepsilon_2}\right)^{1/2}, \tag{2.23}$$

and

$$k_{zi} = \pm\left(\varepsilon_i\left(\frac{\omega}{c}\right)^2 - k_x^2\right)^{1/2}, i = 1,2. \tag{2.24}$$

2.2 The Excitation of Surface Plasmon Polaritons

As shown in Figure 2.3, the surface plasmons modes always lie beyond the light line, indicating it has greater k_x than a free photon of the same frequency. This makes a direct excitation of a surface plasmon mode impossible. There are two methods to excite the surface plasmon polaritons.

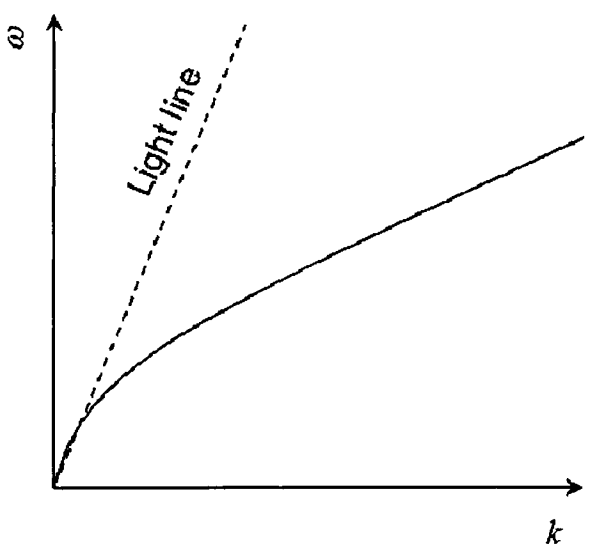

Figure 2.3 The dispersion relation of light (dotted line) and surface plasmon polaritons (solid line). For light, $\omega = kc$, and for surface plasmon polaritons, $\omega = k_x c$.

(a) *Grating Coupler*. If light (k=ω/c) hits a grating with a grating constant s, at an angle θ_s, as shown in Figure 2.4, the component of the incident wave in the surface can be expressed as [64]

$$k_x(out) = k_x(in) \pm MG, \tag{2.25}$$

where $k_x(in) = \frac{\omega}{c}\sin\theta_s$, $G = \frac{2\pi}{s}$ and M is an integer.

According to Eqn. (2.25), the grooves in the grating surface break the translation invariance and allow k_x of the outgoing wave to be different from that of the incoming wave. As a result, the outgoing wave vector is able to match the wave vector of surface plasmon polaritons. Correlated experiments have been reported in reference [65].

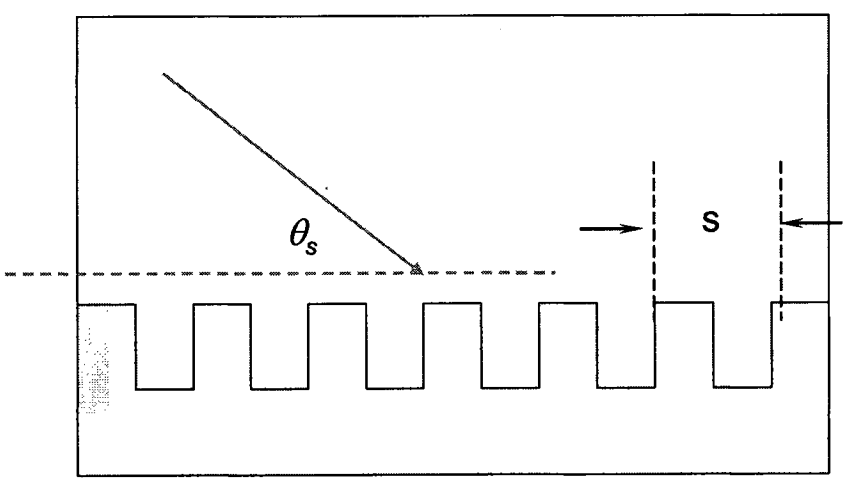

Figure 2.4 The grating coupler for surface plasmon polaritons

(b) *ATR Coupler*. As shown in Figure 2.5 (a), if light is reflected at a metal surface covered with a dielectric medium–glass prism, its wave vector projected on the metal-glass prism surface can be calculated as

$$k_x = \sqrt{\varepsilon_0}\frac{\omega}{c}\sin\theta\,. \tag{2.26}$$

where ε_0 is the permittivity of the glass prism.

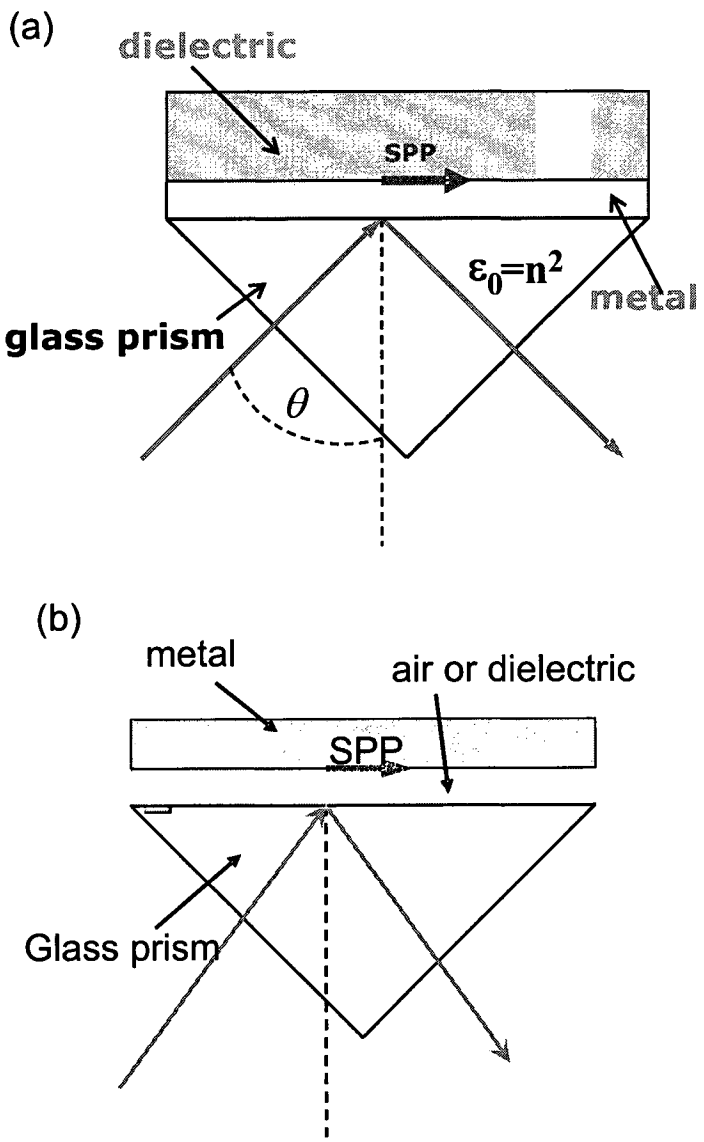

Figure 2.5 Configuration of ATR setups: (a) Kretschmann configuration, (b) Otto configuration.

Thus, the dispersion relation, Eqn. (2.23), can be satisfied. At such conditions, when SPPs get excited, the energy goes from the incident light to the SPPs. Correspondingly, the minimum is observed in the angular dependence of the reflectance.

There are two ATR setups to excite the surface plasmon polaritons, as shown in Figure 2.5. The Otto configuration [66] is shown in Figure 2.5 (b), in which the metal surface is separated by an air or dielectric at a distance of about one wavelength from the glass prism. The setup used in the dissertation is known as Kretschmann setup [67], Figure 2.5 (a), in which the metallic film is directly deposited on the surface of prism.

2.3 The Modeling of the Reflectance of Surface Plasmon Polaritons

The quantitative description of the reflected intensity can be given by Fresnel's equation for the three-layer system 0/1/2 [64]: 0 is dielectric medium; 1 is metallic film with thickness d; 2 is dielectric medium, as shown in Figure 2.6.

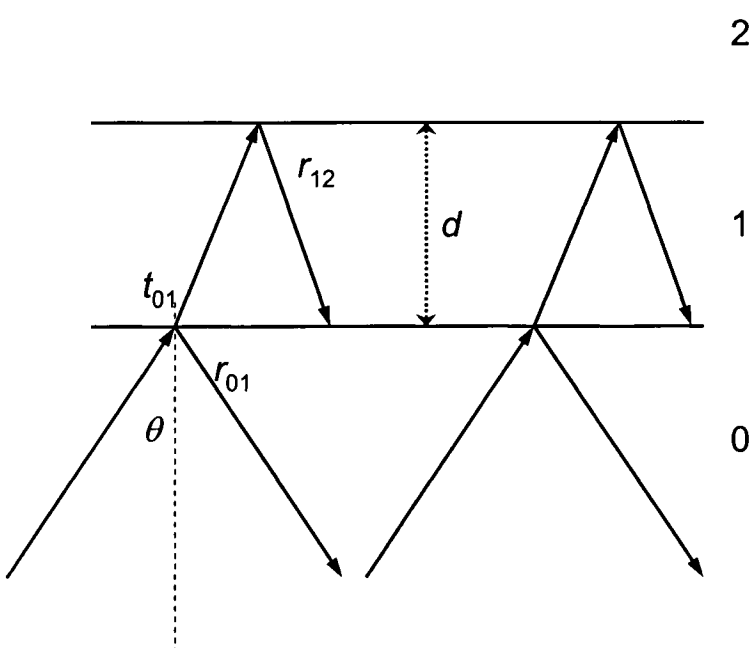

Figure 2.6 Calculation of R in three-layer system

One can calculate the total reflection by using the Maxwell's equations together with the boundary conditions at the two interfaces, between medium 0 and medium 1, and between medium 1 and medium 2, respectively. The light beam is partially reflected by the interface (0/1) and partially transmitted through the interface (0/1) and is back reflected at the interface (1/2), Figure 2.6. The amplitude can be calculated with Fresnel's equations for p-polarized light

$$r_{ik}^{p} = \left(\frac{k_{zi}}{\varepsilon_i} - \frac{k_{zk}}{\varepsilon_k}\right) \Big/ \left(\frac{k_{zi}}{\varepsilon_i} + \frac{k_{zk}}{\varepsilon_k}\right), i,k = 0,1,2. \tag{2.27}$$

and k_{zi} is given by Eq. (2.24), in which the k_x is followed by Eq. (2.31) [65]. Thus,

$$k_{zi} = \pm\left(\varepsilon_i\left(\frac{\omega}{c}\right)^2 - (\sqrt{\varepsilon_0}\frac{\omega}{c}\sin\theta)^2\right)^{1/2}, i = 0,1,2. \tag{2.28}$$

The sum of the reflected beams or the total intensities of the reflected wave comes out as

$$R = \left|\frac{E_r}{E_0}\right|^2 = \left|\frac{r_{01}^{p} + r_{12}^{p}\exp(2ik_{z1}d)}{1 + r_{01}^{p}r_{12}^{p}\exp(2ik_{z1}d)}\right|^2, \tag{2.29}$$

where E_0 and E_r are the incident and the reflected fields, respectively.

Let's go back to glass-metal-dielectric system, Figure 2.5 (b). At the certain value of angle θ_0, known as critical angle, the energy of incident light is transferred to SPPs, Eqn. (2.26), yielding a minimum in the reflectivity profile $R(\theta)$. Here one has

$$k_x^0 = \sqrt{\varepsilon_0}\sin\theta_0 = \sqrt{\frac{\varepsilon_1\varepsilon_2}{\varepsilon_1 + \varepsilon_2}}, \tag{2.30}$$

where the k_x^0 denotes the wave vector at the critical angle.

If one re-writes ε_i as

$$\varepsilon_i \equiv \varepsilon_i^{'} + j\varepsilon_i^{''}, i = 1,2 \tag{2.31}$$

where $\varepsilon_i^{'}$ and $\varepsilon_i^{''}$ are the real and imaginary parts of the dielectric constant of the medium, Eqn. (2.23) can be re-written as:

$$k_x = \frac{\omega}{c}\left[\frac{\left(\varepsilon_1^{'} + j\varepsilon_1^{''}\right)\left(\varepsilon_1^{'} + j\varepsilon_2^{''}\right)}{\left(\varepsilon_1^{'} + \varepsilon_2^{'}\right) + i\left(\varepsilon_1^{''} + \varepsilon_2^{''}\right)}\right]^{1/2} \tag{2.32}$$

One can present the complex wave vector as a sum of its real and imaginary components $k_x = k_x^{'} + jk_x^{''}$. Assuming that $\varepsilon_2^{''}, \varepsilon_1^{''} << \varepsilon_1^{'}, \varepsilon_2^{'}$, one obtains

$$k_x^{'} \approx \frac{\omega}{c}\left(\frac{\varepsilon_1^{'}\varepsilon_2^{'}}{\varepsilon_1^{'} + \varepsilon_2^{'}}\right)^{1/2} \tag{2.33}$$

$$k_x^{''} \approx \frac{\omega}{2c}\left(\frac{\left(\varepsilon_1^{'2}\varepsilon_2^{''} + \varepsilon_2^{'2}\varepsilon_1^{''}\right)}{\left(\varepsilon_1^{'} + \varepsilon_2^{'}\right)\sqrt{\varepsilon_1^{'}\varepsilon_2^{'}\left(\varepsilon_1^{'} + \varepsilon_2^{'}\right)}}\right) \tag{2.34}$$

For real k'_x, we need $\left|\varepsilon'_1\right| > \varepsilon'_2$ since ε'_1 is usually smaller than zero. The imaginary component of the wave vector, k''_x, determines the decay of the SPP due to internal losses, γ_i, which is caused by the absorption in metal and dielectric. Correspondingly, one has

$$k_x^{''} = \gamma_i = \frac{\omega}{2c}\left(\frac{\varepsilon_1\varepsilon_2}{\varepsilon_1 + \varepsilon_2}\right)^{3/2}\left(\frac{\varepsilon_1^{''}}{\varepsilon_1^{2}} + \frac{\varepsilon_2^{''}}{\varepsilon_2^{2}}\right). \tag{2.35}$$

We can see that the internal loss will be compensated by gain in dielectric at

$$\varepsilon_2^{''} = -\frac{\varepsilon_2^{'2}\varepsilon_1^{''}}{\varepsilon_1^{'2}}, \tag{2.36}$$

leading to $k''_x = \gamma_i = 0$.

Eqn. (2.29) is useful for numerical calculation of the reflectivity profile $R(\theta)$ and not convenient for the qualitative analysis. Under several simplifying assumptions, we reduced Eqn. (2.29) to the one, which can be easily understood qualitatively [66].

At the additional assumption that the angles of interest θ are in the vicinity of the critical angle θ_0, Eq. (2.29) can be reduced to [68]

$$R(\theta) \approx |r_{01}|^2 [1 - A - B], \tag{2.37}$$

where

$$A = \frac{4\gamma_i \gamma_r}{(k_x - k_x^0 - \Delta k_x^0)^2 + (\gamma_i + \gamma_r)^2}, \tag{2.38}$$

$$B = \frac{4(k_x - k_x^0 - \Delta k_x^0)\,\mathrm{Im}(r_0)\,\mathrm{Im}(e^{j2k_z^0 d_1})/\xi}{(k_x - k_x^0 - \Delta k_x^0)^2 + (\gamma_i + \gamma_r)^2}. \tag{2.39}$$

Here r_{01}, given by Eqn. (2.27), is the amplitude reflection coefficient at the boundary between glass and metal, and z-components of the wave vectors, k_{zi}, are determined by Eqn. (2.28) at $k_x = k_x^0$.

The term A (Eqn. 2.38) is Lorentzian. An almost similar term was calculated in Ref. [64] under the additional simplifying assumption $\varepsilon_2 = 1$. The width of the Lorentzian function is determined by the sum of the internal loss $\gamma_i \equiv k_x^{0"}$ and the radiative loss

$$\gamma_r = \mathrm{Im}\left(r_{01} e^{j2k_z^0 d_1}\right)/\xi, \tag{2.40}$$

where

$$\xi = \frac{c\left(\varepsilon_2' - \varepsilon_1'\right)}{2\omega}\left(\frac{\varepsilon_2' + \varepsilon_1'}{\varepsilon_2' \varepsilon_1'}\right)^{3/2}. \tag{2.41}$$

The shift of the extremum of the Lorentzian profile from its resonant position determined by $\mathrm{Re}(k_x^0) = (\omega/c)n_0 \sin\theta_0$ is related to the radiative loss and given by the formula

$$\Delta k_x^0 = \mathrm{Re}\left(r_{01} e^{j2k_z^0 d_1}\right)/\xi . \qquad (2.42)$$

The term B in Eqns. (2.38, 2.39) is Lorentzian multiplied by the asymmetry factor $(k_x\text{-}k_x^0\text{-}\Delta k_x^0)$. This term was missing in Ref. [66]. The profiles $R(\theta)$ calculated based on Eqn. (2.37) are almost the same as the one calculated from Eqn. (2.29) [68].

2.4 The Numerical Results

2.4.1 The Basic Calculations of the Reflection Profile

As we show below, the choice of the sign in Eqn. (2.28) plays a key role in the simulation of the reflection profile. The parameter $k_z c/\omega$ defines the field distribution along the z direction. Its real part can be associated with a tilt of phase-fronts of the waves propagating in the media, and is often discussed in the context of positive *vs* negative refractive index materials ([45, 48, 54, 69-74]), while its imaginary part defines the wave attenuation or growth. The sign of the square root in Eqn. (2.28) should be selected to enforce the causal energy propagation. For dielectrics excited in total internal reflection geometry, as well as for metals and other media with $\mathrm{Re}[k_z^2] < 0$, which do not support propagating waves, the imaginary part of the square root should be always positive. For other systems, the selection should enforce the wave decay in systems with loss ($\varepsilon''>0$) and the wave growth in materials with gain ($\varepsilon''<0$) [73]. This physical selection of the sign can be achieved by the cut of the complex plane along the negative imaginary axis.

In detail, when the wave propagates in the glass prism (i = 0), the sign of square root in Eqn. (2.28) should be obviously picked as positive.

When i = 1, indicating that the waves propagates in the system only involved glass prism and metal, since ε''_1 is always positive (propagation with absorption), the sign of square root in Eqn. (2.28) has to be positive as well.

When i = 2, the choice of the sign in Eqn. (2.28), which is rather obvious in the case of positive ε_2'', becomes not trivial when ε_2'' is negative. When the complex value $\kappa = k_{z2}{}^2 = \kappa' + j\kappa''$ is described by a vector pointing to the first quadrant of the imaginary-real plane, the choice of the sign of the square root in Eqn (2.28) is trivial: the sign is positive and the complex value k_{z2} belongs to the first quadrant, which corresponds to the wave propagation with absorption.

When the complex vector κ corresponds to the second quadrant, the solution is also quite obvious: k_{z2} still belongs to the first quadrant, with the phase angle φ limited as $\pi/4 < \varphi < \pi/2$. This is the case of the evanescent field with a very small propagating component. In the limiting case of a very weak absorption, when κ' is negative, κ'' is positive and $|\kappa'| >> |\kappa''|$, the phase angle φ approaches $\pi/2$ and the field becomes almost purely evanescent.

When the system is lightly pumped to produce a very small amount of gain, the sign of κ'' changes to negative and $|\kappa'|$ is still much larger than $|\kappa''|$. At some very weak pumping, κ'' passes through zero, which corresponds to a purely evanescent field, k'_{z2}=0. We argue that by passing from small absorption to small gain, the solution for the wave vector k_{z2} does not experience any discontinuity, and when κ belongs to the third

quadrant, k_{z2} belongs to the second quadrant with the phase angle φ limited by $\pi/2 < \varphi < 3\pi/4$, Figure 2.7. If, instead, we would pick the root for the wave vector k_{zi} (the one pointing to the fourth quadrant), then at the minimal value of the gain the solution would correspond to the maximal amplification of the propagating wave, which in this case will have a very small real component of the wave vector. This solution appears to be completely unphysical: that is why we choose the square root as it is shown in Figure 2.7.

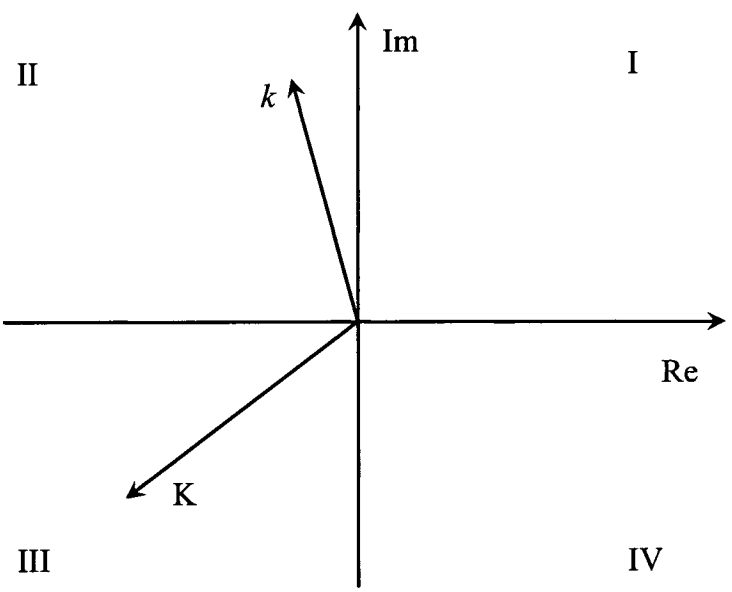

Figure 2.7 Choice of the solution of Eqn. (2.28) in the case of negative ε''

When the complex vector κ points to the fourth quadrant, the solution appears to be trivial again: the wave vector k also belongs to the fourth quadrant, which corresponds to the propagating wave with amplification.

Although such cut of the complex plane is different from the commonly accepted cuts along the positive [74] or negative [45, 48, 69-71, 73] real axes, our simulations

(Figure 2.8) show that this is the only solution guaranteeing the continuity of measurable parameters (such as reflectivity) under the transition from a weak loss regime to a weak gain regime. More importantly, our selection is the only one consistent with previous results on gain-assisted reflection enhancement, predictions of gain-assisted SPP behavior [52-54, 56], and our experimental data described below.

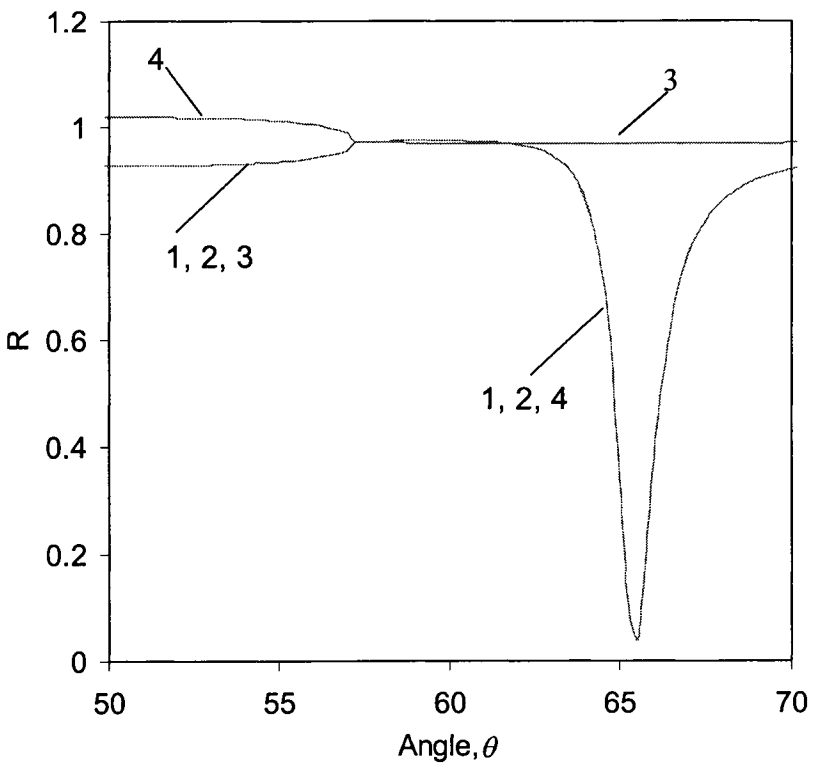

Figure 2.8 Numerical results of R(θ). For all data sets: ε_1=-15.584+0.424j, d_1=50 nm, and λ=594 nm. Trace 1: dielectric with very small loss, ε_2=2.25+10^{-5}j. Traces 2-4: dielectric with very small gain, ε_2=2.25-10^{-5}j. Trace 2: complex cut along negative imaginary axis (correct; nearly overlaps with trace 1). Trace 3: complex cut along positive real axis; Trace 4: complex cut along negative real axis.

Figure 2.8 shows the only correct way to pick up the right sign in Eqn. (2.28) in the case of with and/or without the presence of gain. In all the calculations ε_0 = 1.7835^2=3.18173, ε_1 = -15.584+0.424 j, ε_2 = 2.25+$10^{-5}j$ or ε_2 = 2.25-$10^{-5}j$, λ=594 nm and d = 50 nm. As shown in Figure 2.8, if the complex cut is along the negative imaginary axis, there is no discontinuity from small positive ε''_2 (loss) to small negative ε''_2 (gain). However, if the cut is along the positive real axis or the negative real axis, the calculated results are obviously incorrect, in contradiction to the experimental result in Figure 2.8.

Note that active media excited above the angle of total internal reflection, as well as the materials with ε'<0 and ε''<0 formally fall into the negative index materials category. However, since $|k_z''|$ in this case is greater than $|k_z'|$, the "left handed" wave experiences very large attenuation (in the presence of gain!!!), which in contrast to claims of Ref. [71], makes the material unsuitable for super-lenses and other proposed applications of NIMs [45, 48, 68-70].

2.4.2 Numerical Results of the Reflection Profile Without Gain

The profiles of the reflectivity $R(\theta)$ were calculated at the wavelength λ= 594 nm for a broad range of values of gain and metal thickness.

We calculated the dependencies $R(\theta)$ for the dielectric medium ε_2 being air, Figure 2.9, and polymethylmethacrylate (PMMA) doped with Rhodamine-6G (R6G) dye, Figure 2.10, at different thicknesses of silver ranged from 0nm to 90nm. The index of refraction of PMMA/R6G was taken to be equal to 1.5. In the model, the metal was silver, which dielectric constant was calculated using the data published in Ref. [75]. At the resonance

(critical) angle θ_0, the energy of incident light was transferred to SPPs, yielding a minimum in the reflectivity profile $R(\theta)$, as shown in Figures 2.9 and 2.10.

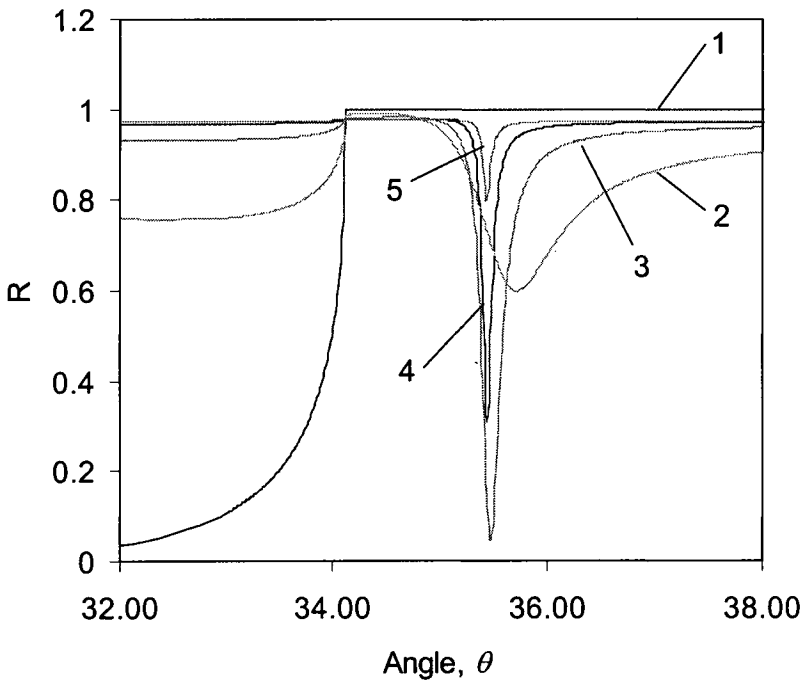

Figure 2.9 Reflectance profiles $R(\theta)$ calculated for silver films of different thicknesses. The parameters used in the calculations are ε_0=3.180872 (glass), ε_1=-15.584+0.424j (silver at λ=594 nm), ε_2=1 (air). Trace 1 - 0 nm, Trace 2 - 30 nm, Trace 3 - 50 nm, Trace 4 - 70 nm, Trace 5 - 90 nm.

The results show that the $R(\theta)$ profile has a broad 'dip' about its minimum value for thin metal films (≤30nm). However, the dip in the $R(\theta)$ profile narrows and deepens in relatively thick films (≥50nm). The dip remains narrow but shallow at very thick metal films (≥90nm), Figures 2.9 and 2.10.

There is a significant shift in the angular position of the dip when the dielectric medium is changed from air (Figure 2.9) to R6G/PMMA (Figure 2.10). This result is in accord with Eqn. (2.30) and is known in the literature Ref [64]. At the same time, the shape of the profile $R(\theta)$ does not change much with the change of the dielectric.

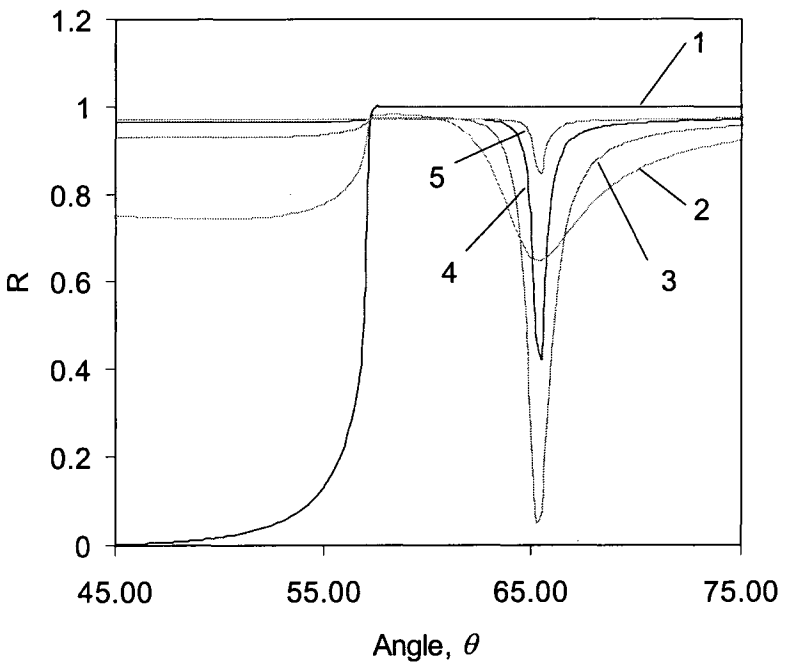

Figure 2.10 Reflectance profiles $R(\theta)$ calculated for silver films of different thicknesses with R6G-PMMA as a dielectric medium. The parameters used in the calculation are ε_0=3.180872 (glass), ε_1=-15.584+0.424j (silver at λ=594 nm), ε_2= 2.25 (PMMA with small concentration of R6G, such that the imaginary part of the dielectric constant can be neglected). Trace 1 - 0 nm, Trace 2 - 30 nm, Trace 3 - 50 nm, Traces 4 - 70 nm, Trace 5 - 90 nm.

2.4.3 Theoretical Modeling of the Reflection Profile With Gain

The calculated dependencies of R against angle θ for different values of ε_2'' (gain) were plotted to determine how large a gain is needed to compensate for loss due to absorption in metal, Figure 2.11.

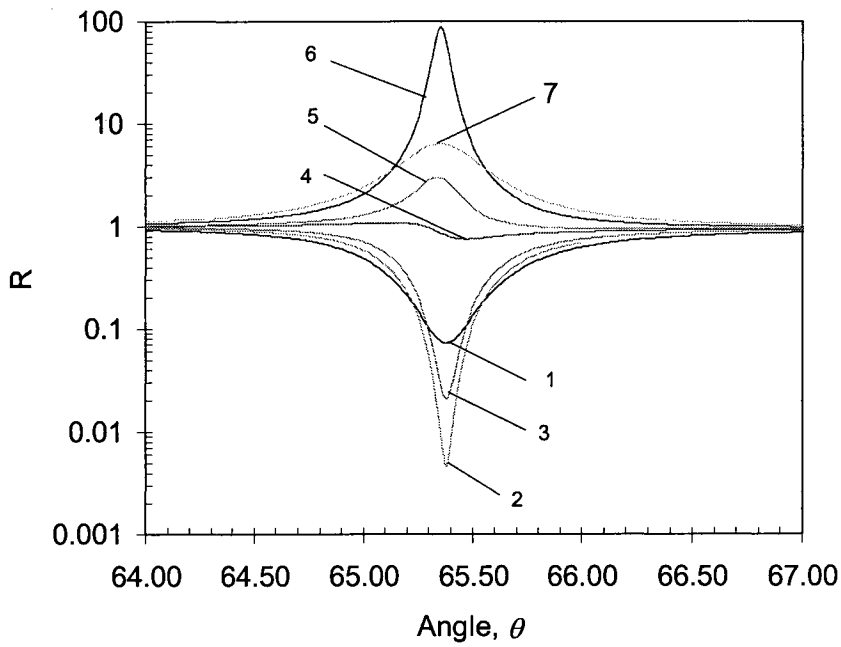

Figure 2.11 Reflectance profiles R(θ) calculated for silver films with R6G-PMMA as a dielectric medium in the presence of different gain. The parameters used in the calculation are λ=594 nm , d= 60nm, ε_0=3.180872 (glass), ε_1=-15.584+0.424j, and ε_2= 2.25+ε''_2j. Trace 1 - ε''_2=0, trace 2 - ε''_2=-0.003, trace 3 - ε''_2=-0.005, trace 4 - ε''_2=-0.0085, trace 5 - ε''_2=-0.01, trace 6 - ε''_2=-0.0148, trace 7 -ε''_2=-0.02.

At zero level of the gain, the profile $R(\theta)$ calculated for a 60 nm metal film has a relatively broad "dip". With the addition of gain, the internal loss γ_i becomes smaller, and the "dip" in the dependence $R(\theta)$ narrows and becomes deeper. With further increase in

the absolute value of ε_2'' , the dependence $R(\theta)$ becomes deeper, until the minimal value R_{min} reaches zero, which corresponds to the gain where the internal loss is equivalent to the radiative loss, shown in Eqns. (2.37-2.39).

With the further increase of gain, the loss γ_i continues to decrease, and the dip is getting more shallow and asymmetric. At some larger negative value of ε_2'', when gain compensates internal loss in the metal, Eqn. (2.36), the value of $R(\theta)$ is equal to 1. In the immediate vicinity of γ_i=0, the term A is much smaller than the term B and the reflectivity profile $R(\theta)$ is highly asymmetric, Figure 2.12 (trace 4).

With further increase in the absolute value of ε_2'', the dip in the reflection curve $R(\theta)$ turns to a peak, which grows to an infinitely high value when the gain compensates for both radiative and internal losses. The reflectivity R greater than unity does not violate any conservation laws because the dielectric medium has to be pumped in order to maintain negative ε_2''.

Past the peak point, Eqns. (2.29) and (2.37) predict the reduction of the reflectivity, as shown in Figure 2.11 (trace 7). However, this situation is probably unphysical, since one cannot maintain a steady-state gain in an infinitely large amplifying system assumed in our model. In order to adequately describe the system with high values of gain, one should consider the system of rate equations describing populations of energy states of dye as well as a coupling between excited molecules and the SPP field.

The reflection minima and maxima are plotted versus ε_2'' for silver films at different thicknesses, d, in Figures 2.12. Not surprisingly, the value of gain at which R crosses one does not depend on d because internal loss is determined by the materials'

constants only, as shown in Eqn. (2.36). For the thick film, with increase in the absolute value of ε_2'', the "dip" in the dependence R (θ), firstly narrows, then becomes deeper and at some point reaches zero. With the further increase of ε_2'', the dip turns to a peak gradually, just as described above. Note that when the thickness of the silver film is small (<50 nm), there is no initial decrease of reflection. Instead, the minimal value of R increases starting from the smallest negative values of ε_2''.

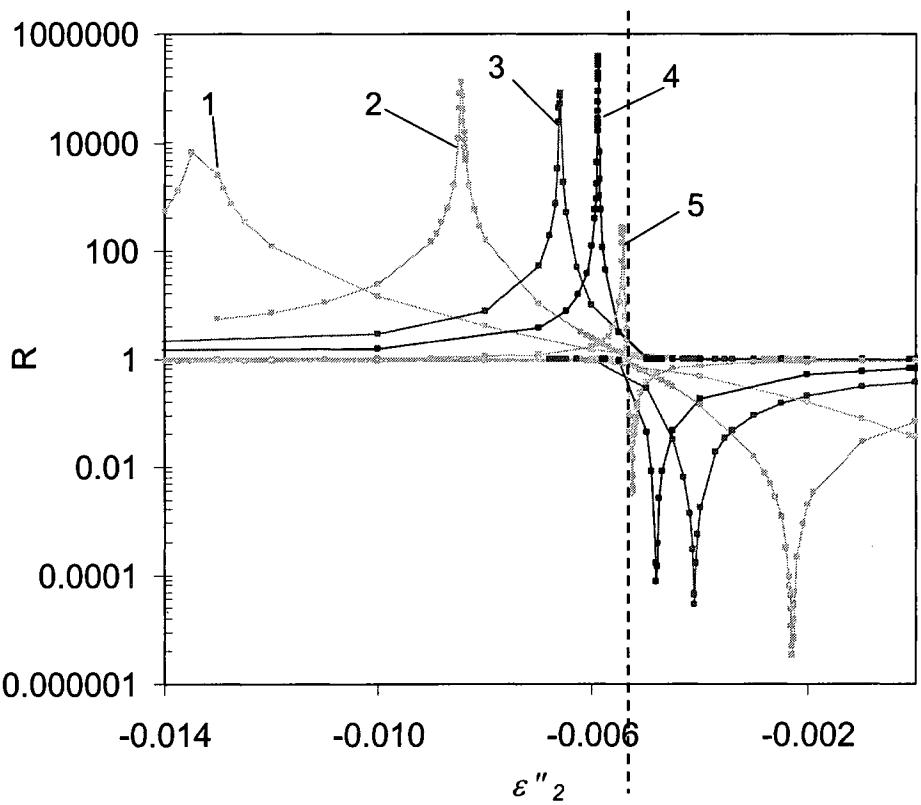

Figure 2.12 The minima and maxima of reflection are plotted versus ε_2'' for different thicknesses of silver film. Trace #1 - 50nm; trace #2 - 60nm; trace #3 - 70nm; trace #4 - 80nm; trace #5 - 100nm. When the values of ε_2'' cross -0.0054 (dot line), which is independent on the thicknesses of silver film, the value of R cross one.

The width W of the dip or peak of the $R(\theta)$ is plotted as a function of ε_2'' shown in Figure 2. 13. The width W decreases nearly linearly with the increase of the negative value of ε_2" and reaches zero at the singularity point determined by $\gamma_i+\gamma_r=0$, when the *total* SPP loss is compensated by gain.

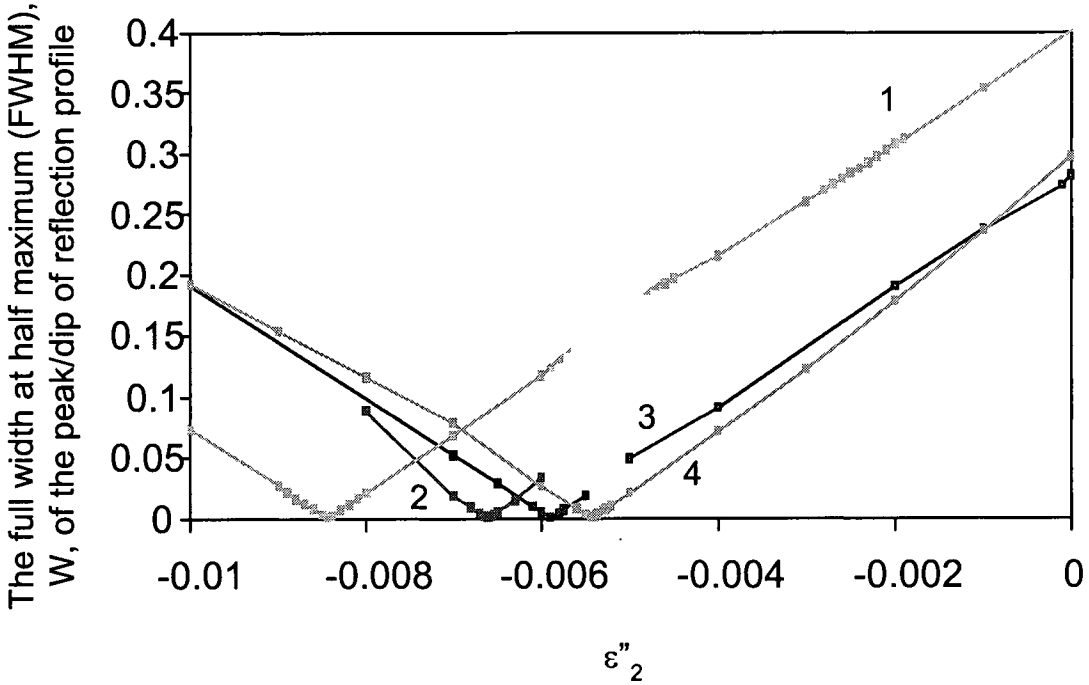

Figure 2.13 The full width at half maximum (FWHM) of the dip or peak of the reflectivity profile R(θ) as a function of the value of gain, negative ε_2''. Trace #1 - 60nm; trace #2 - 70nm; trace #3 - 80nm; trace #4 - 100nm.

At the same point, the propagation length L of the SPP given by

$$L = [2(\gamma_i + \gamma_r)]^{-1} \tag{2.46}$$

becomes infinitely long. According to Ref. [68], L^{-1} is equal to the inverse propagation length of SPP obtained directly by solving Maxwell equations in a multilayered system. Thus the width ΔW of the reflectivity profile $R(\theta)$ reveals the total loss in the system $\gamma_i+\gamma_r$ and the length of the plasmon propagation L. One can see that with the increase of gain (increase of the negative value of ε_2''), the width of the profile gradually decreases and reaches zero when gain compensates for the *total* loss. Thus, by increasing the amount of gain in a dielectric medium, one can infinitely elongate the propagation length of the surface plasmon.

Chapter 3

ELONGATION OF SURFACE PLASMON POLARITONS PROPAGATION LENGTH WITHOUT GAIN

In this Chapter, it is demonstrated through experiment that the addition of highly concentrated rhodamine 6G chloride dye to the PMMA film adjacent to a silver film can cause 30% elongation of the propagation length of surface plasmon polaritons (SPPs). The possibility to elongate the SPP propagation length without optical gain opens a new technological dimension to low-loss nanoplasmonic and metamaterials.

3.1 Background

It is well known that two metals commonly used in nanoplasmonic and metamaterials applications are silver and gold. Silver has a smaller absorption loss, and gold is a better technological material. Unfortunately, the propagation length of SPP in these metals (in the visible range) is of the order of ten micrometers or shorter.

The known solution to the loss problem is optical gain added to a dielectric medium, as discussed in Section 1.3. In spite of significant progress made in this direction, maintaining required optical gain (of the order of 10^3 cm^{-1}) is a technologically difficult task, which often requires a Q-switched laser [60]. This makes the gain solution to solve the loss problem unpractical for many applications. Ideally, one would want to have a low loss in passive systems, without any gain.

Can metal-dielectric interfaces be improved to become more suitable for photonic applications? In silver, there is a significant difference between the experimentally measured absorption loss in the visible and ultraviolet ranges of the spectrum and that predicted by the Drude model, which takes into account the contribution of free electrons only [76]. By the first principles calculations, it has been shown that this difference is due to bound electrons in the layers of silver atoms adjacent to the metal surface. This is evidenced by Figure 3.1, comparing the experimental absorption loss with that calculated in bulk silver and silver slabs of different thicknesses [77].

Transitions between occupied *d* states and empty *s* states (or hybridized *s* and *p* states) at or above the Fermi level dominate in the ultraviolet absorption, and hybridized *s-p* states contribute to absorption in the visible range of the spectrum. Correspondingly, by changing the Fermi level of a metallic layer or modifying surface states of bound

electrons, one can, in principle, reduce absorption at a specific wavelength, possibly by shifting the absorption band to some other wavelength unimportant for a particular application.

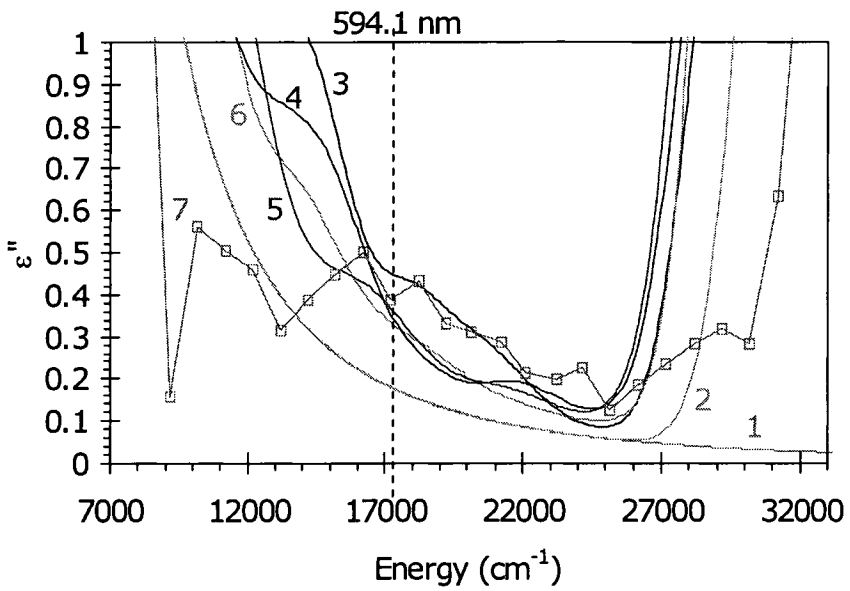

Figure 3.1. Imaginary part of the dielectric constant of silver ε" calculated (1) according to the Drude model with plasma frequency ω_p=9.1 eV and loss parameter Γ=0.021 eV; (2) from the first principles for bulk silver; (3-6) for the (1,1,1) surface of silver slabs consisting of 7, 10, 13, and 16 monolayers. Trace 7 - experimental data [77].

According to Refs. [78, 79], *n*-doping of noble metals (alloys of noble metals with metals, which donate two or three electrons per atom to a free electron gas) can increase the Fermi level and, correspondingly, shift bound state absorption to higher frequencies. Thus, adsorption of molecules, ions or radicals onto the silver surface can modify surface electronic states and reduce the absorption loss of silver. This effect was demonstrated in

Ref. [80], where adsorption of oxygen on Ag(110) removed the effect of surface states and substantially reduced optical response around 1.7 eV (730 nm, 13700 cm^{-1}).

In this work, following the ideas outlined above, we have demonstrated elongation of the SPP propagation length by bringing silver film in contact with the PMMA film heavily doped with rhodamine 6G chloride dye.

3.2 Experimental Samples and Setup

Experimentally, we have studied SPPs in the attenuated total reflection (ATR) setup, which is discussed in Chapter 2. 2.

The 90^0 glass prisms were cleaned rigorously with methanol, acetone and de-ionized water for a total time of 15 to 20 minutes before the deposition of the metal film.

Depositions of metal films on prisms from pieces of silver ingots were done using the BOC Edwards Auto 306 vacuum coater. The prisms with the deposited films were cooled in the vacuum for 25-30 minutes to prevent chemical oxidation of the metal film. The gauge in the vacuum coater gives approximate values of the thickness of the deposited metal film. However, more accurate thickness measurements were done using the Veeco Dektak-6M profilometer. The thickness of the silver film in different samples varied between 35 and 72 nm.

Rhodamine 6G chloride dye (R6G) and polymethyl methacrylate (PMMA) were dissolved in dichloromethane. The solutions were applied to the surface of silver and dried in air, providing a PMMA film doped with R6G. The thickness of the PMMA film was ~10 μm and the concentration of R6G varied between 0 and 100 g/l ($2.1x10^{-1}$ M).

In the experiment, SPP was excited at the silver-R6G/PMMA interface with the He-Ne laser operating at λ= 594 nm (*p* polarized), Figure 3.2. A chopper operating at 125 Hz was set in the incoming laser beam. The film-coated prism was mounted on a motorized goniometer.

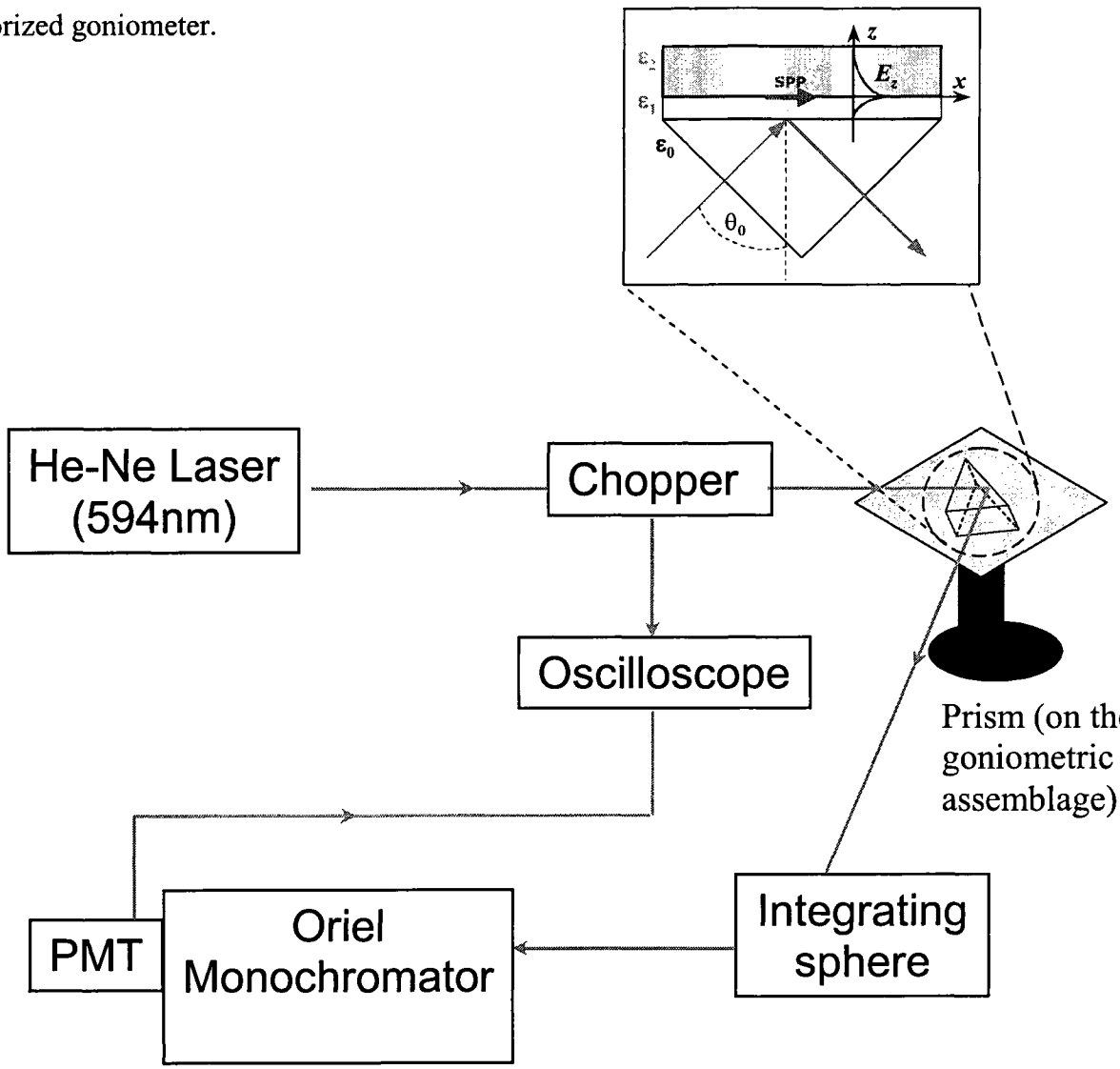

Figure 3.2 Schematic diagram of the setup for the surface plasmon polariton measurement without pumping (gain)

The illuminated spot on the back side of the prism was positioned on the axis of rotation of the goniometer. This helps to keep the illuminated spot steady when the prism is rotated.

Reflected light from the hypotenuse side of the film-coated prism was collected via an integrating sphere and a bundle of optical fibers, Figure 3.2, into the input slit of the Oriel MS257 monochromator. The monochromator was set at the wavelength $\lambda = 594$ nm. The optical signal was converted into the electronic signal by the photomultiplier tube (PMT). The electronic signal from the PMT was sent by a 1GHz Tektronix oscilloscope. In some measurements, a lock-in amplifier was also used to detect and record the PMT signal. Using this setup, by slowly rotating the goniometer, we were able to record the angular dependence of reflectivity $R(\theta)$.

3.3 Experimental Results

The absorption spectra of PMMA/R6G films featured a characteristic band centered at 530nm. Typical absorption spectrum of PMMA/R6G films is shown in Figure 3.3.

At high concentration of dye, its long-wavelength wing significantly increased in comparison to that recorded at low concentration of R6G. The imaginary part of the dielectric constant of the PMMA/R6G film, ε_2'', can be calculated as

$$\varepsilon_2'' = \frac{\lambda k_{abs}}{4\pi}. \qquad (3.1)$$

where k_{abs} is the absorption co-efficient, cm^{-1}, and λ is the wavelength.

From the absorption data, the value of ε_2'' at $\lambda = 594$ nm is calculated and plotted as a function of concentration of R6G (in *log-log* scale) in Figure 3.4.

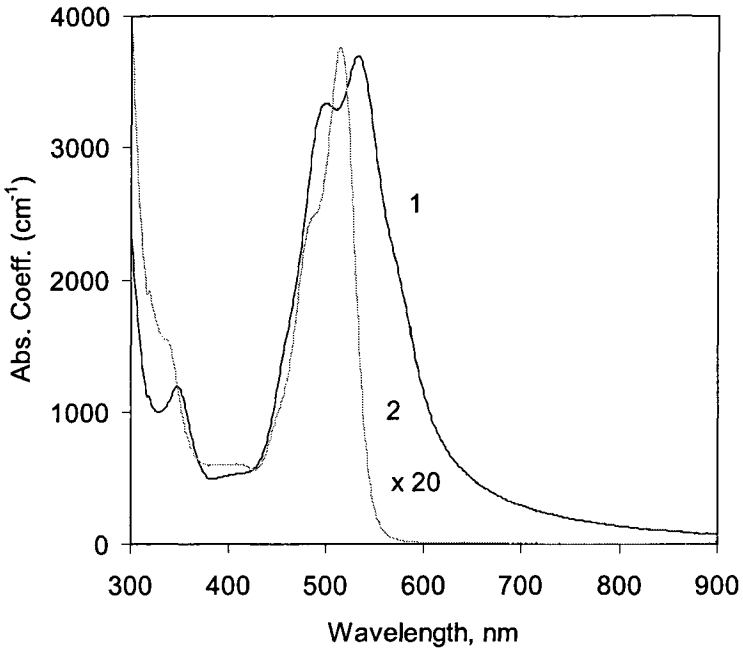

Figure 3.3 Absorption spectrum of PMMA film doped with R6G; trace 1 – 100 g/l; trace 2 – 5 g/l

At high concentration of dye, the slope of the curve approached 2, which indicated dimerization of dye molecules. Large scatter of the data was due to known relatively low reproducibility of PMMA/R6G films.

We started reflectivity experiments with measuring the angular profile $R(\theta)$ in pure glass prism, without any deposited films, as shown in Figure 3.5. By fitting the function $R(\theta)$ with Eqn. (2.29) at d=0 and ε_2=1, we determined the index of refraction of glass $n_0 = (\varepsilon_0)^{1/2}$ to be equal to 1.7835 at 594 nm, in a very good agreement with the data provided by the manufacturer.

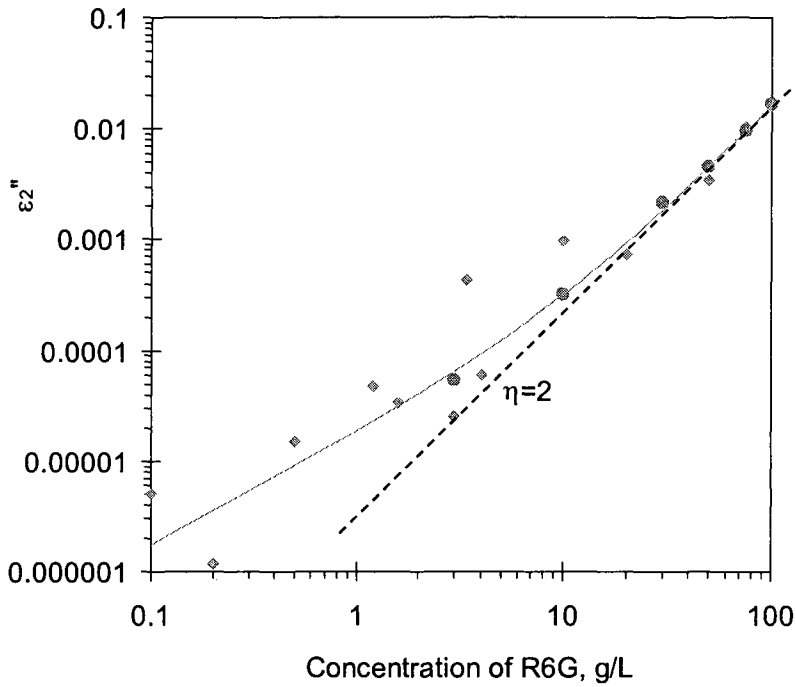

Figure 3.4 Imaginary part, ε_2", of the dielectric constant of the PMMA/R6G film as a function of concentration of R6G. Diamonds: data calculated from the absorption measurements. Solid line: data points ε_2" fitted with a second order polynomial. Dotted line has the slope equal to η=2. Circles: the values ε_2" used at the fitting of the R(θ) profiles in glass/silver/polymer structures.

We then repeated the same measurements with the PMMA/R6G films (with different concentrations of R6G dye) deposited directly onto the prism. One of the $R(\theta)$ with the R6G concentration equal to 30 g/L is shown in Figure 3.6 (a). The rear surfaces of the polymeric films were intentionally roughened to prevent the reflection of light from the polymer/air interface back to the prism. Each reflectivity profile $R(\theta)$ was fitted with Eqn. (2.29) at d=0 to determine the dielectric constant of the PMMA/R6G film. The real part of dielectric constant of PMMA/R6G films as a function of the concentration of R6G was shown in Figure 3.6 (b).

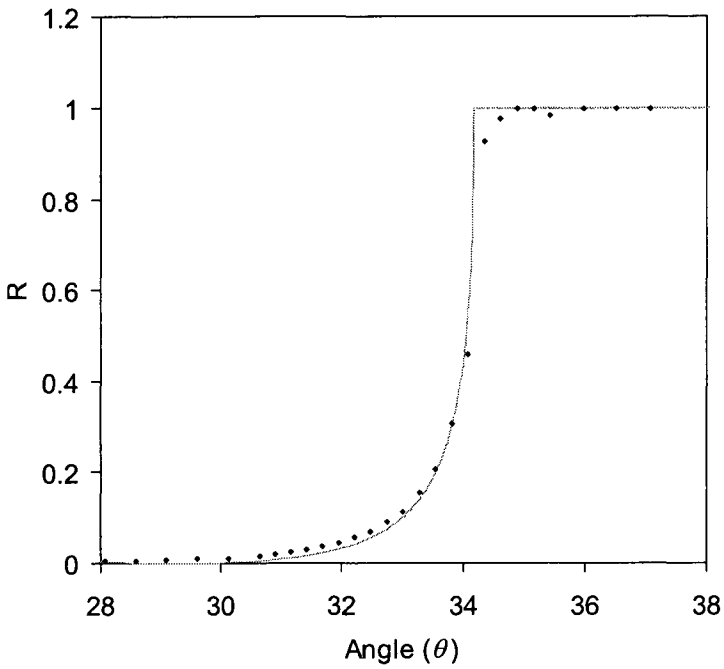

Figure 3.5 Solid line, numerical result of R(θ) with $\varepsilon_0=1.735^2$, d=0 nm, $\varepsilon_2=1+10^{-31}j$(air), and λ=594 nm. Dots, Angular dependence of the reflectivity R(θ) recorded in the setup of Fig. 3.2 of glass prism.

The reflectivity studies carried out in three-layer structures (glass/silver/polymer) at different concentrations of dye resulted in profiles $R(\theta)$ characteristic of SPPs, Figure 3.6. The reflectivity profile $R(\theta)$ had a characteristic dip at the angle at which the wave vector of the SPP matched the projection of the photon wave vector to the plane of metal-dielectric interface. Here it is assumed that each of the three media (glass/silver/polymer with dye) is spatially uniform, the boundaries between media are sharply defined and effects of hybrid states at the interfaces are neglected.

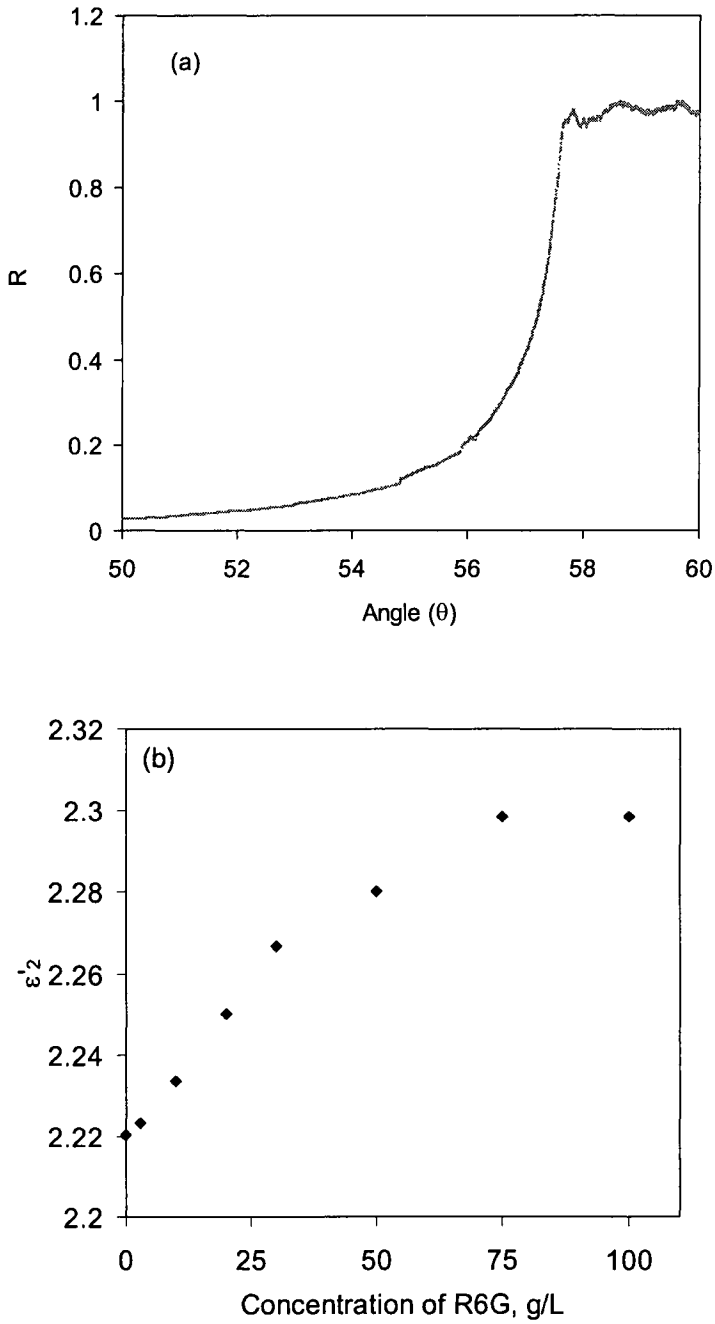

Figure 3.6 (a) Angular dependence of the reflectivity R(θ) recorded in the setup of Fig. 3.1 of glass prism coated with PMMA/R6G film. The concentration of R6G is 30 g/L; (b) Real part of the dielectric constant ε_1' of PMMA/R6G as a function of R6G concentration.

As shown in Figure 3.7, the most remarkable result of this measurement is that the width W of the dip of the angular profile $R(\theta)$ decreased with an addition of R6G to PMMA, up to the concentration of dye $N \approx 30$ g/l, and then increased again when the concentration of dye was increased further. According to Ref. [60], W is inversely proportional to the SPP propagation length L. Correspondingly, the obtained experimental result implies that an addition of R6G dye to PMMA helps to reduce the loss and elongate the propagation length of SPPs.

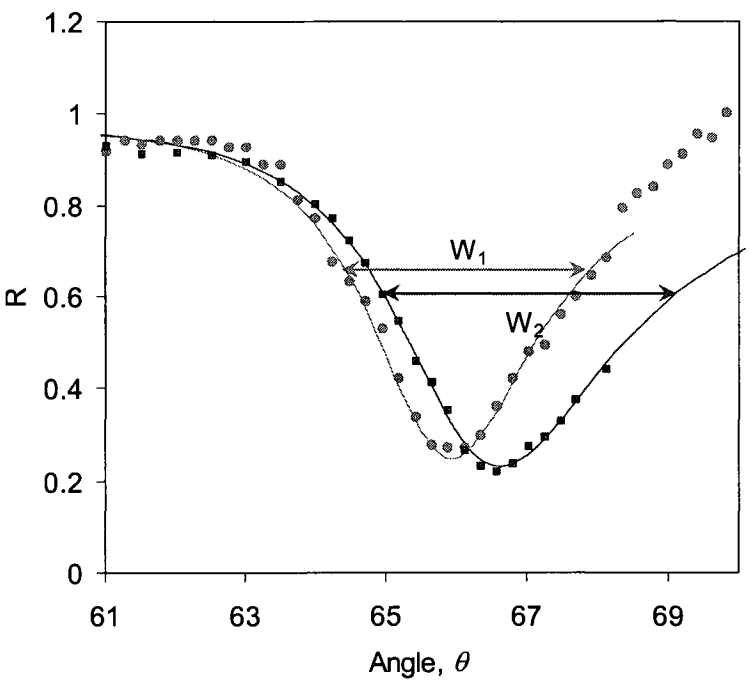

Figure 3.7 Angular dependence of the reflectivity R(θ) recorded in the setup of Fig. 3.1, with the concentration of the R6G dye equal to 0 g/l (squares) and 30 g/l (circles). With the addition of dye, the width of the reflectivity profile decreased and the position of its minimum shifted.

We then fitted the reflectivity profiles $R(\theta)$ using Eqn. (2.29), with the fitting parameters being real and imaginary parts of the dielectric constant of silver, ε_1' and ε_1'', and imaginary part of the dielectric constant of PMMA/R6G, ε_2''. The experimental features to fit were the angular position of the dip in the dependence $R(\theta)$, its width and depth, as well as the reflectivity profile below the angle of total internal reflection. Given experimental traces which were so rich with characteristic signature features (Figure 3.6), we could extract from the fitting the three parameters above with high degree of confidence. This way determined the real and imaginary parts of the dielectric constant of silver (at λ=594 nm), ε_1' and ε_1'', are plotted against the concentration of R6G in Figure 3.8 (a) and (b).

In the absence of R6G, the value of ε_1' coincided within 5% with those published in Refs. [75, 81]. The value of ε_1'' was smaller than that in Ref. [81] and larger than that in Ref. [75]. The obtained ε_2'' from fitting imaginary parts of the dielectric constant of PMMA/R6G were in good agreement with those directly measured in the absorption experiment shown in Figure 3.4.

Both extracted values ε_1' and ε_1'' were strongly influenced by the presence of R6G dye in the PMMA film, Figure 3.8 (a) and (b). A particularly strong effect – threefold reduction – has been observed in the dependence ε_1'' of the concentration of R6G with the increase of the concentration of dye from 0 g/l to 100 g/l. This implies that in a framework of a simple model, assuming that each of the three media is spatially uniform, the boundaries between media are sharply defined and the effects of hybrid states at the interfaces are neglected, this gigantic reduction of ε_1'' would be required to account for the change in the SPP propagation length observed experimentally.

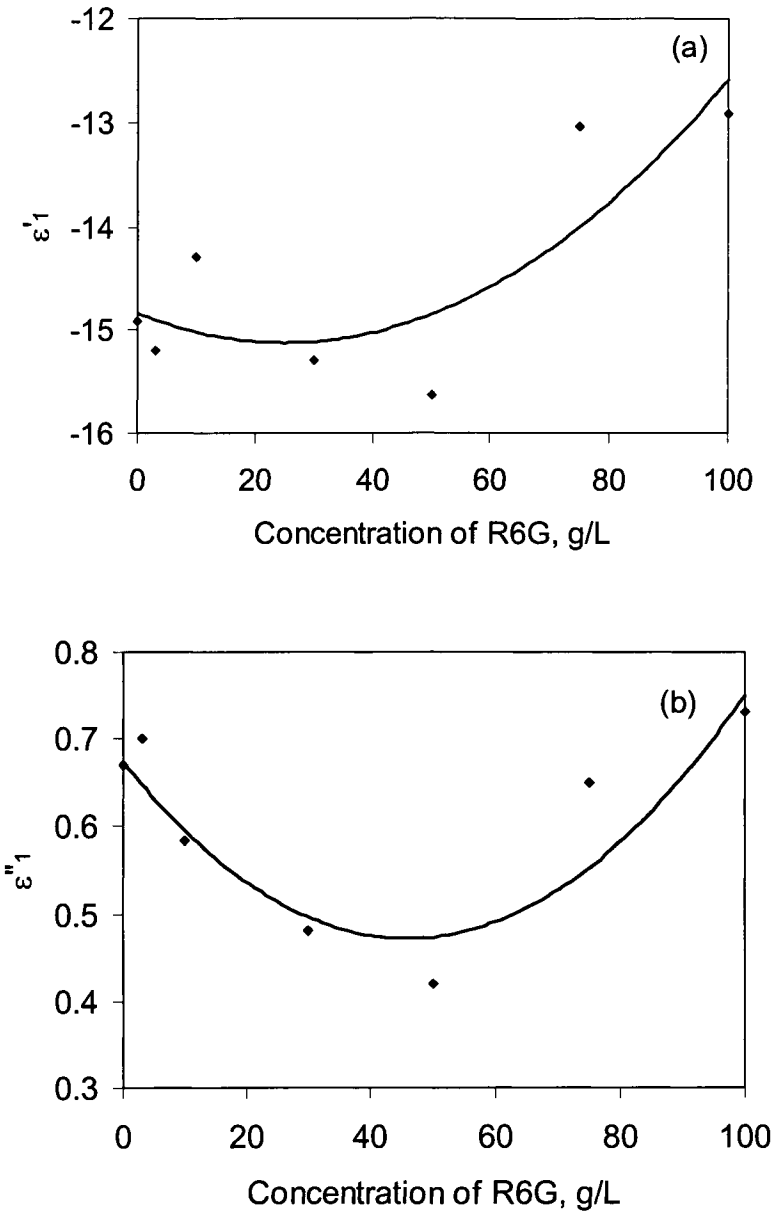

Figure 3.8 Obtained from the fitting of R(θ) real (a) and imaginary (b) parts of the dielectric constant of silver, ε_1', as a function of the R6G concentration N. Solid lines – interpolations with second order polynomials.

3.4 Discussion

The propagation length L of SPPs can be calculated according to Eqn. (2.46) [77]. In order to calculate the dependence $L(N)$ for two different thicknesses of the metallic film, d_1=40 nm and d_1=80 nm (Figure 3.8), we substituted to Eqn. (2.46) functions $\varepsilon_1(N)$ and $\varepsilon_2(N)$ obtained by extrapolation of the experimental data in Figs. 4-8 with second order polynomials. Because the values of the radiative loss γ_r and, correspondingly, the SPP propagation lengths L are different at d_1=40 nm and d_1=80 nm, the two data sets $L(N)$ were normalized to unity at N=0 for convenience of presentation.

The fact that that the two normalized curves $L(N)$ (calculated at d_1=40 and d_1=80 nm) nearly overlap each other suggests that the *relative* change of the SPP propagation length with the concentration of dye is not strongly dependent on the thickness of the silver film. This justifies the comparison of the calculated values $L(N)$ with the inverse widths W^{-1} of the reflectivity profiles $R(\theta)$ measured in different samples with the thickness of the silver film varying between 35 and 72 nm, Fig. 3.9.

Not surprisingly (since W^{-1} is proportional to L [68]), these two types of curves closely resemble each other, confirming ~30% elongation of the SPP propagation length with the increase of the dye concentration to N=30 g/l ($6.3\text{x}10^{-2}$ M).

The monotonous reduction of ε_1'' with the increase of N, depicted in Fig. 3.7 (a), suggests that the SPP propagation length should continuously increase with the increase of dye concentration. The reduction of L with the increase of N above 30 g/l is primarily due to the increase of the absorption loss ε_1'' in the PMMA/R6G film with the increase of N, Fig. 3.8 (b). Figure 3.9 demonstrates the strong difference between the values of L calculated under the assumption of ε_2''=0 (no loss in dielectric) and at the experimental

values of ε_2". The second cause for the reduction of L at high values of N is the increase of ε_1', which becomes less negative.

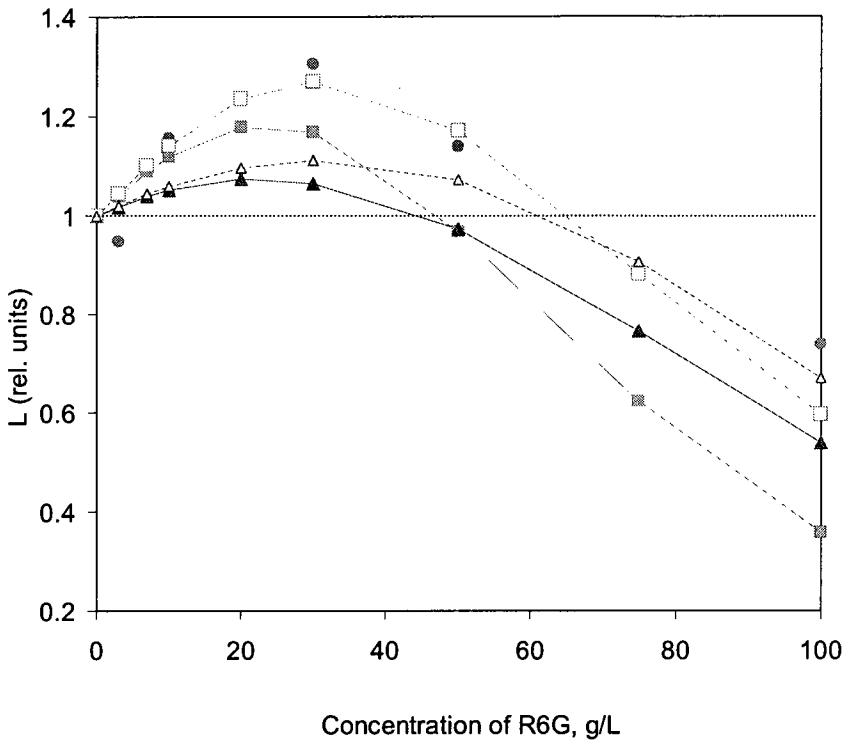

Figure 3.9 SPP propagation length L as a function of dye concentration N. Solid squares (triangles) – calculations done for real experimental parameters at d_1=80 nm (40 nm); Open squares (triangles) – calculations done for the hypothetical case of the absence of dye absorption, ε_2"=0, at d_1=80 nm (40 nm). Solid circles – inverse width of the reflectivity profile R(θ). All data sets are normalized to unity at N=0.

Along with the heuristic models discussed in the beginning of this chapter, we tentatively explain the change in ε_1" with one of the following reasons: (1) electron transfer occurring between PMMA/R6G and silver and the corresponding shift of the Fermi level in a thin surface layer of Ag (~1 nm) to which electric charge propagates and

(2) modification of electronic states in silver layer adjacent to the metal-dielectric interface, including possible formation of the AgCl phase. Both possibilities are currently under investigation, and the findings of the comprehensive studies will be reported elsewhere [79].

The preliminary results of *ab initio* modeling show that the formation of AgCl film can, indeed, affect the absorption loss at the surface [77]. Using the cyclic voltammetry technique, we reconstructed the energy level diagram of $R6G^+$ radical with the reference to the vacuum level. Its comparison with the energy diagram of silver did not indicate that any efficient electron transfer involving $R6G^+$ radicals could be possible. At the same time, negatively charged chlorine ions (Cl^-) appear to be a more plausible source of electrons.

3. 5 Summary

To summarize, we have demonstrated that the addition of highly concentrated rhodamine 6G chloride dye to the PMMA film adjacent to the silver film causes 30% elongation of the propagation length of SPP without gain. This opens a new technological dimension to low-loss nanoplasmonics and metamaterials, in which surface phenomena and hybrid electronic states play an enormously important role in determining physical properties of nanocomposites and nanostructures.

Chapter 4

COMPENSATION OF LOSS BY OPTICAL GAIN IN PROPAGATING SURFACE PLASMONS POLARITONS

The compensation of loss of *propagating* SPPs at the interface between silver film and optically pumped polymer with dye is reported in this chapter. The level of gain achieved in our experiments ($\approx$ 420 cm^{-1} at λ=594 nm) is, in principle, sufficient to compensate the propagation loss of SPPs in high-quality silver films. As a result, the large magnitude of the effect, nearly threefold change of the reflectivity, enables a variety of applications of 'active' nanoplasmonics.

4.1 Introduction

The interaction between active materials and SPPs has been a focus of theoretical and numerical research for several decades. The field-matching approach was employed in Ref. [54] to calculate the reflectivity during plasmon excitation in an attenuated total internal reflection (ATR) geometry; the authors of Ref. [52] have proposed that the optical gain in a dielectric medium can elongate the SPP's propagation length; gain-assisted excitation of resonant SPPs has been predicted in [56]; SPP propagation in active waveguides is described in [55], and the group velocity modulation of SPPs in nano-waveguides has been discussed in [82]. The possibility to influence *propagating* surface plasmons by optical gain in an adjacent dielectric medium has been demonstrated in Ref. [57].

In Ref. [57], an amplification of surface plasmons at the interface between a flat continuous silver film and a liquid containing organic dye molecules was demonstrated experimentally. The experimental setup, which was first proposed by Sudarkin's group [52], in Ref. [57], is shown in Figure 4.1 (a). The dye is optically pumped by a dye laser operating at $\lambda = 580$ nm, creating a population inversion in the dye molecules, which then act to deliver energy to the plasmon field by stimulated emission. A p-polarized probe light at $\lambda = 633$ nm to excite the plasmon to be amplified enters the prism through opposite faces. A flow cell with circulating dye is attached to the side of the prism carrying the metal film, which is important for preventing the photobleaching, and for reducing the heat load caused by absorption of the pump light. The angular differential reflection curves obtained experimentally and theoretically for various thicknesses of the silver film are illustrated in Figure 4.1(b). As followed by Figure 4.1(b), for a film thickness around 40nm, the

reflectance change induced by the amplifying medium is positive across the whole reflected dip, which is in agreement with our theoretical prediction, Chapter 2.4 (Figure 2.12).

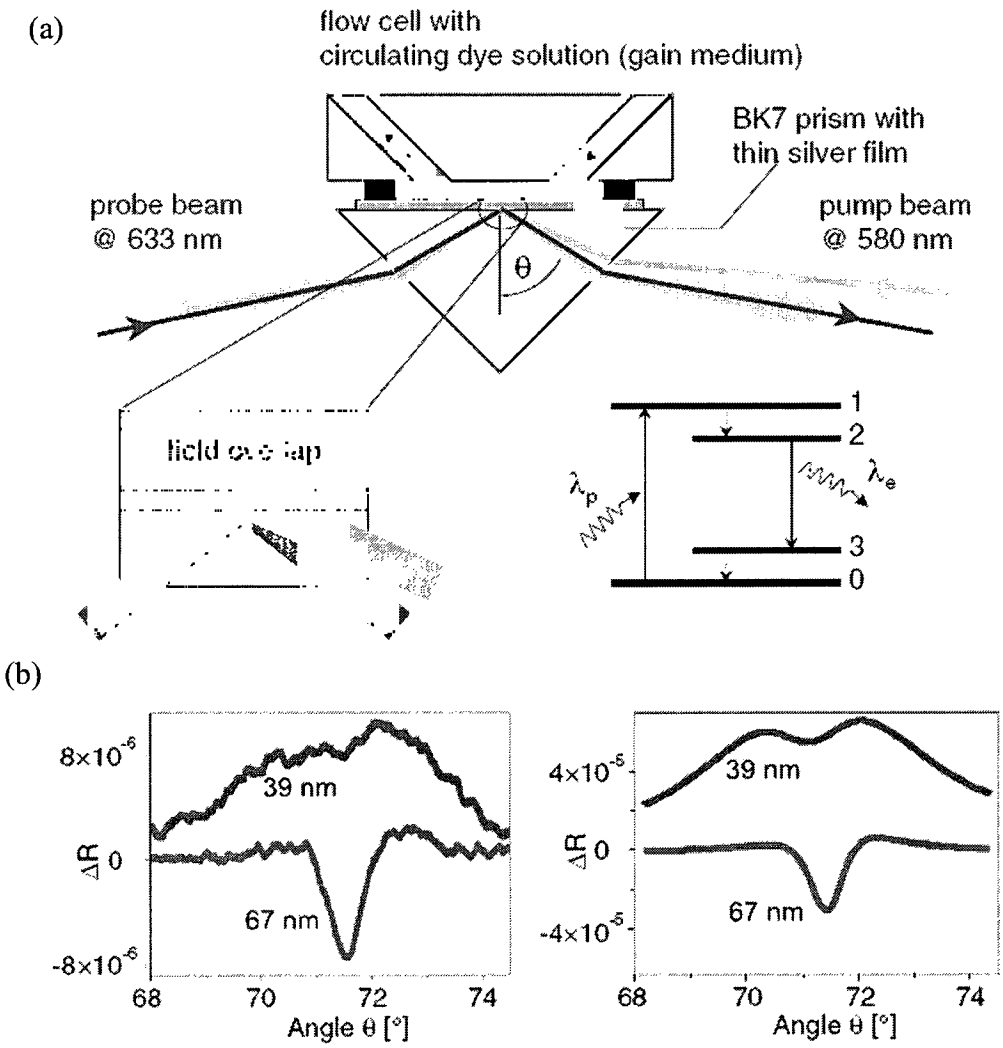

Figure 4.1 (a) The Twin ATR method for surface plasmon polaritons amplification; (b) Differential reflectance curves as a function of angle for different metal film thicknesses. Left, experimental results; Right, calculated results [57].

At large thickness around 65nm, the induced reflection change is negative, which indicates a deepening of the reflectance dip. Again, this result is also predicted in Chapter 2.4 (Figure 2.13).

However, the observed change of reflectance induced by gain Ref. [57] is as small as 0.001%, because the provided gain is relatively weak. If more efficient materials, and/or pumping methods are developed, a large amplitude change of reflection will be observed. This might lead to the further application of nanoplasmonics.

4.2 Experimental Setup and Samples

Experimentally, SPPs were studied in the attenuated total internal reflection setup. The 90° prism was made of glass with the index of refraction n_0=1.784. Metallic films were produced by evaporating 99.99% pure silver in the vacuum evaporator. The PMMA/R6G films were obtained by the method described in Chapter 3. In the majority of experiments, we used the concentration of dye equal to 10 g /L (2.1×10^{-2} M) and the polymer film thickness of the order of 10 μm.

In this work, the experimental setup, similar to the one described in Chapter Three, was shown in Figure 4.2. A frequency doubled radiation of the Q-switched Nd: YAG laser (Quanta Ray, λ=532 nm, t_{pulse}=10 ns, repetition rate 10 Hz) was used to optically pump the R6G-PMMA film adjacent to the silver covered prism.

The pumping light, which spot diameter (~ 3 mm), was a little bit larger than that of the probe He-Ne beam, was launched to the R6G-PMMA film from outside of the prism, nearly normally to its surface. The pumping beam was aligned to overlap with the He-Ne illuminated spot. Pumping at different light intensities was done by firing single shots of the pump light.

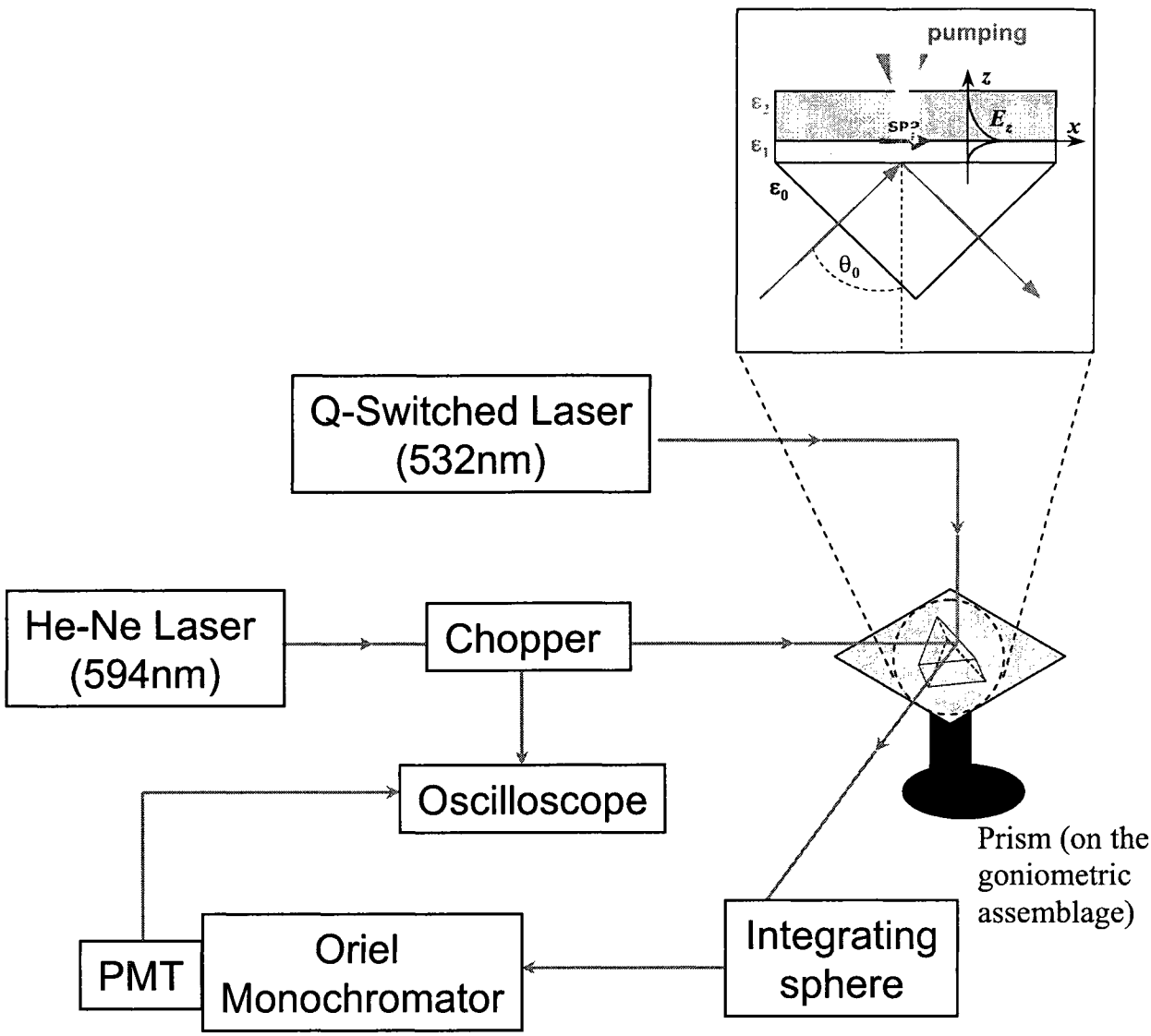

Figure 4.2 Schematic diagram of the setup for the pump-probe experiment

The He-Ne beam reflected from the film-coated side of the prism was diverged by a set of mirrors, through a filter (depending on the intensity of pump light used) to the input slit of the Oriel MS257 monochromator. The slit size of the monochromator was about 0.25mm. The relatively narrow slit was used to reduce the amount of R6G emission.

Neutral density filters were used as needed. In the presence of ~10 ns pumping pulse, we observed a spike (or dip) in the reflectivity kinetics. The emission of R6G contributed to this signal. Thus, to separate the reflectivity from any unwanted contributions, we detected four kinetics for each experimental point:

(1) In the presence of 594 nm He-Ne probe and 532 nm Nd:YAG pumping,

(2) In the presence of 532 nm pump only,

(3) In the presence of 594 nm He-Ne probe only, and

(4) Without any optical signal (electronic background).

4.3 Experimental Results

The typical angular dependence $R(\theta)$ measured in the presence of silver film is shown in inset of Fig. 4.3. From the fitting of the experimental curves $R(\theta)$ with Eq. (2.29), we determined dielectric constants of the deposited silver, ε_1' and ε_1", which, as a rule, did not coincide with those of Ref. [75]. The parameters used in the calculation are ε_0=3.180872 (glass), ε_1= -15+0.85j, ε_2= 2.25+1.906x10^{-4}j. Thus, the values ε_1" in some of our samples were as twice as large as those of Ref. [75].

The intrinsic loss ε_1" in freshly deposited silver films increased with time, possibly because of the oxidation of silver. That is why polymer films were deposited on the top of metallic films as soon as the experimental conditions permitted (typically within one hour after the deposition of silver). When the silver film was sandwiched between glass and R6G/PMMA film, its properties were preserved for a week or longer.

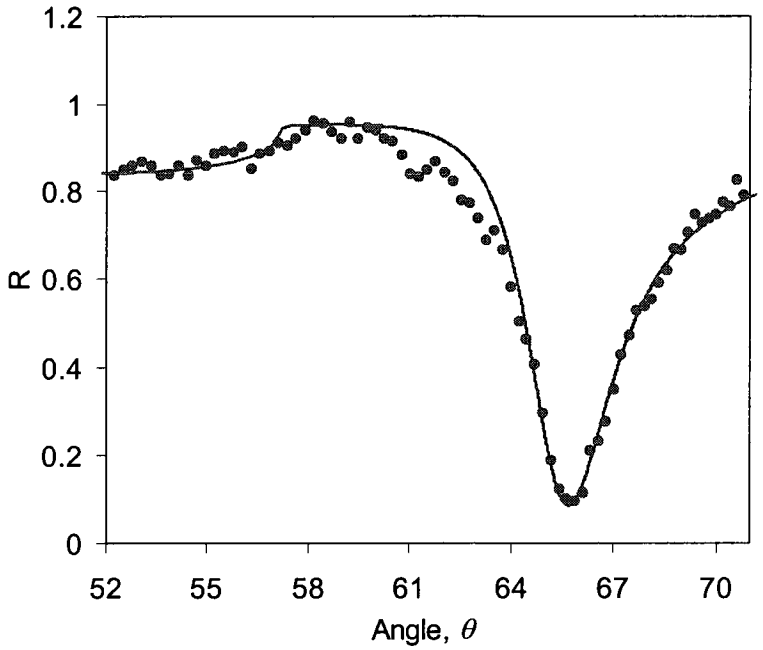

Figure 4.3 Angular reflectivity profile R(θ) recorded in the setup, Figure 4.2 without pumping (spherical dots) and its fitting with Eqn. (2.29) (solid line)

The typical reflectivity kinetics detected at $\lambda = 594$ nm under the 532 nm Q-switched pumping is shown in Figure 4.4.

In samples with relatively thin ($\approx$ 40 nm) metal films, a strong emission signal from the R6G-PMMA film was observed in the absence of He-Ne probe beam. We therefore performed two measurements of kinetics for each data point: one in the absence of the probe beam, and one in the presence of the beam. The spike represents the peak value of the reflectivity during pumping, and the "flat" regions of the kinetics trace correspond to the reflectivity before and after the pumping. We then subtracted "emission background" (measured without He-Ne laser) from the combined reflectivity and emission signal. The

kinetics measurements had a relatively large data scatter, which was partially due to the instability of the Nd:YAG laser.

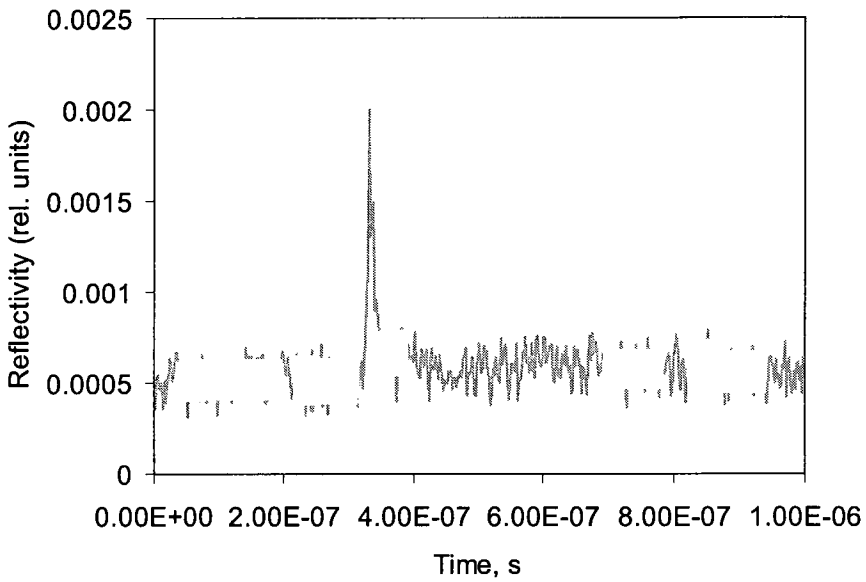

Figure 4.4 Reflectivity kinetics recorded in the glass-silver-R6G/PMMA structure under pumping. The angle θ corresponds to the minimum of the reflectivity, Figure 4.3. Spike in graph represent reflectivity under pumping while flat regions represent reflectivity before and after pumping. The signal has been subtracted from the luminescence.

In the sample with the thickness of the silver film equal ~40 nm, the values of the reflectivity before and during the pumping (16 mJ) were measured at different angular positions of the prism θ, Figure 4.5. The circles in Figure 4.5 correspond to the reflectivity without pumping. Triangles in the Figure 4.5 correspond to the reflectivity measured during the pumping pulse excited to the sample. By dividing the values of R measured in the presence of gain to those without gain, we calculated the relative enhancement of the reflectivity signal to be as high as 280% - a significant improvement in comparison to Ref. [57], where the change of the reflectivity in the presence of gain

did not exceed 0.001%. Fitting the reflectivity curve formed by the triangles with Eqn. (2.29) and known ε'= -15, ε''=0.85 and ε_2' =2.25, yields $\varepsilon_2''\approx$-0.006.

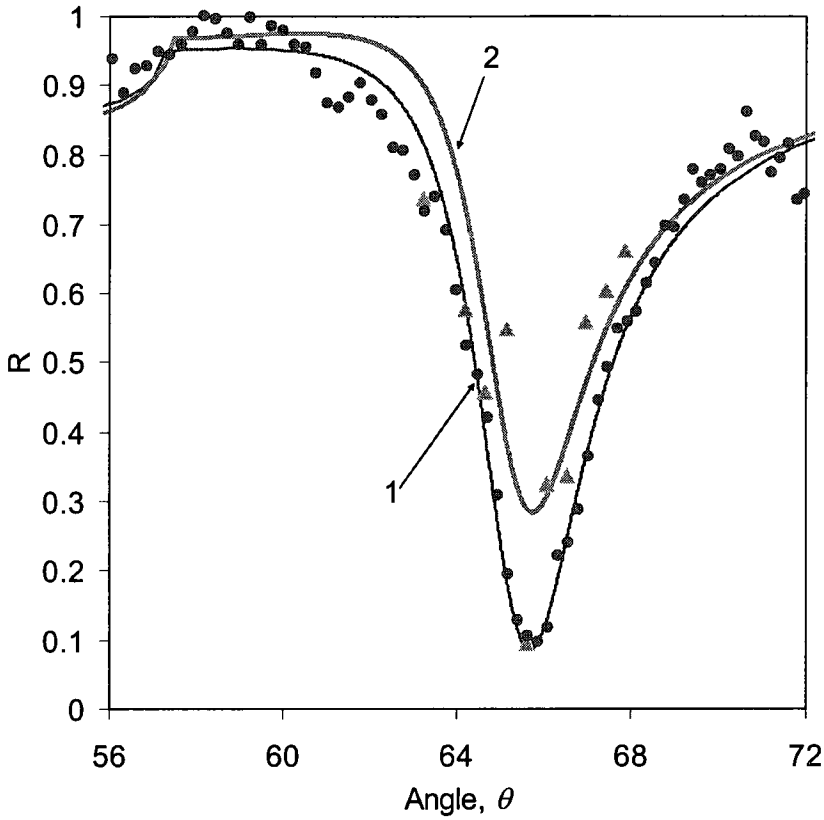

Figure 4.5 The angular reflectivity profile R(θ) recorded in the setup, Figure 4.2, without pumping (circles) and with pumping (triangles). Solid line calculation results according to Eqn. (2.29). ε_0=3.180872, ε_1= -15+0.85j, ε_2= 2.25+ε_2"j. Trace #1-ε_2"= 1.906x10^{-4}, Trace #2-ε_2"= -6.0x10^{-3}.

Followed by the idea of Eqn. 3.1, the following equation is defined to calculate the gain,

$$g = -4\pi \frac{\varepsilon_2''}{\lambda} \tag{4.1}$$

For λ=594 nm, $\varepsilon_2''\approx$-0.006 corresponds to optical gain of g = 420 cm^{-1}.

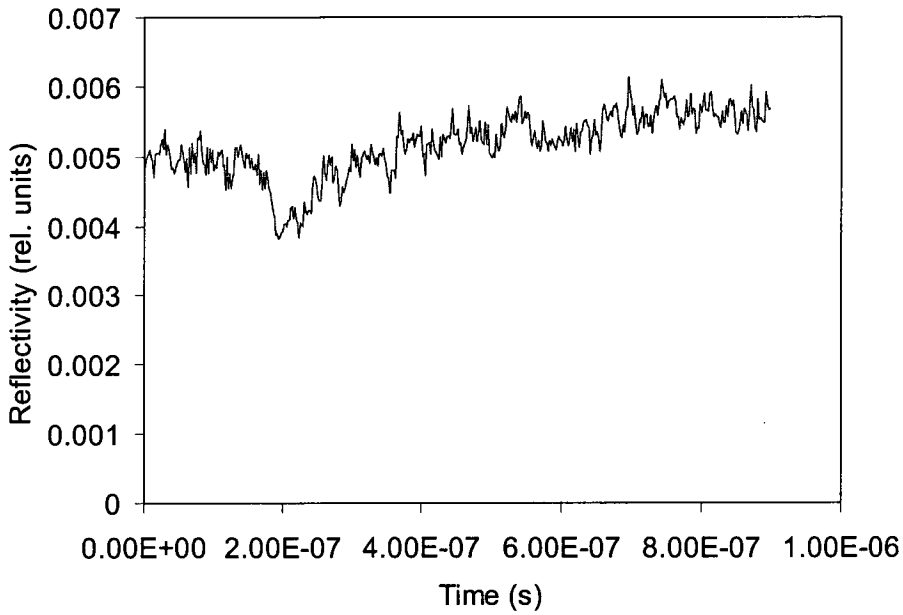

Figure 4.6 Reflectivity kinetics recorded in a thick film (d_1=90 nm) shows a 'dip' at small values of gain.

In thicker silver films, calculations predict initial reduction of the minimal reflectivity $R(\theta)$ at small values of gain followed by its increase (after passing the minimum point R=0) at larger gains, Figure 2.13. The predicted reduction of R was observed in the 90 nm thick film, where instead of a peak in the reflectivity kinetics, we observed a dip, Figure 4.6.

4.4 Discussion

For the silver film parameters measured in our experiment, Eqn. (2.36) predicts complete compensation of *internal* SPP loss at optical gain of g = 1310 cm^{-1}. For a better quality silver characterized by the dielectric constant of Ref. [75] the critical gain is smaller, equal to g=600 cm^{-1}. In addition, if a solution of R6G in methanol (n = 1.329) is used instead of the R6G/PMMA film, then the critical value of gain is further reduced to g = 420

cm^{-1}. This is the value of gain achieved in our experiment. Thus, in principle, at the available gain, one can fully compensate the *internal* SPP loss in silver.

For complete compensation of plasmonic loss in the system, one must also compensate radiation losses. The huge gain of g = 4090 cm^{-1} is required to completely compensate attenuation of SPP in the 40 nm thick film used in our experiment. This value is dramatically reduced in thicker metallic films, since radiative loss strongly depends on film thickness. For relatively thick (≥100 nm) metallic films, *total* loss is almost identical to *internal* ones.

In the experiment described above, the concentration of R6G molecules in the PMMA film was equal to 1.26×10^{19} cm^{-3} (2.1×10^{-2}M). Using the spectroscopic parameters known for the solution of R6G dye in methanol and neglecting any stimulated emission effects, one can estimate that 18 mJ laser pulses used in the experiment should excite more than 95% of all dye molecules. At the emission cross section equal to 2.7×10^{-16} cm^2 at λ=594 nm, this concentration of excited molecules corresponds to a theoretically achievable gain of g=3220 cm^{-1}. The nearly eight-fold difference between this value and the one obtained in our experiment is probably due to the combined effects of luminescence quenching of R6G due to dimerization of rhodamine 6G molecules occurring at a high concentration of dye [83], and amplified spontaneous emission (ASE). While the detailed study of the ASE-induced effects in the R6G/PMMA-silver systems is beyond the scope of this work, we note that at the value of gain equal to g=420 cm^{-1} and the diameter of the pumped spot equal to 3 mm, the optical amplification is enormously large. Obviously, these giant values of the amplification and the gain cannot be maintained in a cw regime, and ASE appears to be a detrimental factor controlling the gain in the pulsed

regime. Correspondingly, the choice of a more efficient amplifying medium (as was proposed in Ref. [57]) may not help in compensating the SPP loss by gain.

4.5 Summary

To summarize, we have demonstrated the optical gain in the dielectric (PMMA film with R6G dye) equal to g=420 cm^{-1}, yielding nearly threefold increase of the resonant value of the reflectivity. In the case of thick low-loss silver film characterized by the dielectric constant of Ref. [75] and low index dielectric, the demonstrated value of gain is sufficient for compensation of the total loss hindering the propagation of surface plasmon polaritons.

Chapter 5

STIMULATED EMISSION OF SURFACE PLASMON POLARITONS

In this work, laser-like emission of surface plasmon polaritons decoupled to the glass prism in an attenuated total reflection setup was observed. SPPs were excited by optically pumped molecules in a polymeric film deposited on the top of the silver film. Stimulated emission was characterized by a distinct threshold in the input-output dependence and narrowing of the emission spectrum. The observed stimulated emission and corresponding to it compensation of the metallic absorption loss by gain enables many applications of metamaterials and nanoplasmonic devices.

5.1 Introduction

Photonic metamaterials, engineered composites with unique electromagnetic properties, have become in recent years a hot research topic because of their interesting physics and exciting potential applications. Localized surface plasmons (SPs) and propagating surface plasmon polaritons (SPPs) play a key role in the design of a majority of metamaterials.

Unfortunately, in contrast to mid- and far-IR structures [84, 85], the performance of optical SP- and SPP-based systems is fundamentally limited by absorption loss in metal, which causes a reduction of the quality factor of SPs and shortening of the propagation length of SPPs.

The solution to the loss problem, which has been proposed over the years in a number of publications [52, 55, 56, 58], is to add an optical gain to a dielectric adjacent to the metal. A substantial enhancement by optical gain of localized SPs in aggregated silver nanoparticles, evidenced by six-fold increase of the Rayleigh scattering, was demonstrated in [60]. A principle possibility to offset SPP loss by gain has been experimentally shown in Ref. [57]; and the optical gain ~ 420 cm^{-1} sufficient to compensate ~30% of the SPP internal loss in a silver film was achieved in Ref. [60].

Here we report experimental observation of the stimulated emission of SPPs at optical frequency. The study in this Chapter proves that the compensation of SPP loss by gain is, indeed, possible, opening the road for many practical applications of nanoplasmonics and metamaterials. Besides resolving one of the fundamental limitations of modern nanoplasmonics, the observed phenomenon adds a new emission source to the "toolbox" of active optical metamaterials.

5.2 Fabrication and Experimental Measurements

In this work, 39 nm - 81 nm silver films were deposited on the glass prism with the index of refraction $n_0 = \sqrt{\varepsilon_0} = 1.7835$ and coated with 1 μm - 10 μm polymethyl methacrylate (PMMA) films doped with rhodamine 6G (R6G) dye in concentration 2.2×10^{-2}M. The same dye-doped polymer was used as a gain medium of random laser in Ref. [86].

Four different sets of experiments have been performed.

(1) In the first set of measurements, used primarily for calibration purposes, we excited SPPs from the bottom of the prism and measured the reflectivity of the sample R as a function of the incidence angle θ, Figure 5.1 (a). As described in the chapters 3 and 4, at the resonance angle θ_0, the energy of incident light was transferred to SPPs, yielding a minimum in the reflectivity profile $R(\theta)$. The $R(\theta)$ (trace 1) in Figure 5.2 is probed at λ =575nm from OPO. The $R(\theta)$ (trace 1) in Figure 5.4 is probed at λ =632.8 nm from He-Neon laser. This standard experiment accompanied by theoretical modeling allowed us to determine the dielectric constants of particular silver films studied.

The width of the reflectivity profile $R(\theta)$ corresponds to the propagation length of SPP, $L = [2(\gamma_i + \gamma_r)]^{-1}$, with γ_i and γ_r being, respectively, intrinsic losses due to material absorption and radiation losses due to SPP decoupling to the prism.

In the remaining experiments, the samples were excited from the PMMA side at a nearly normal angle of incidence.

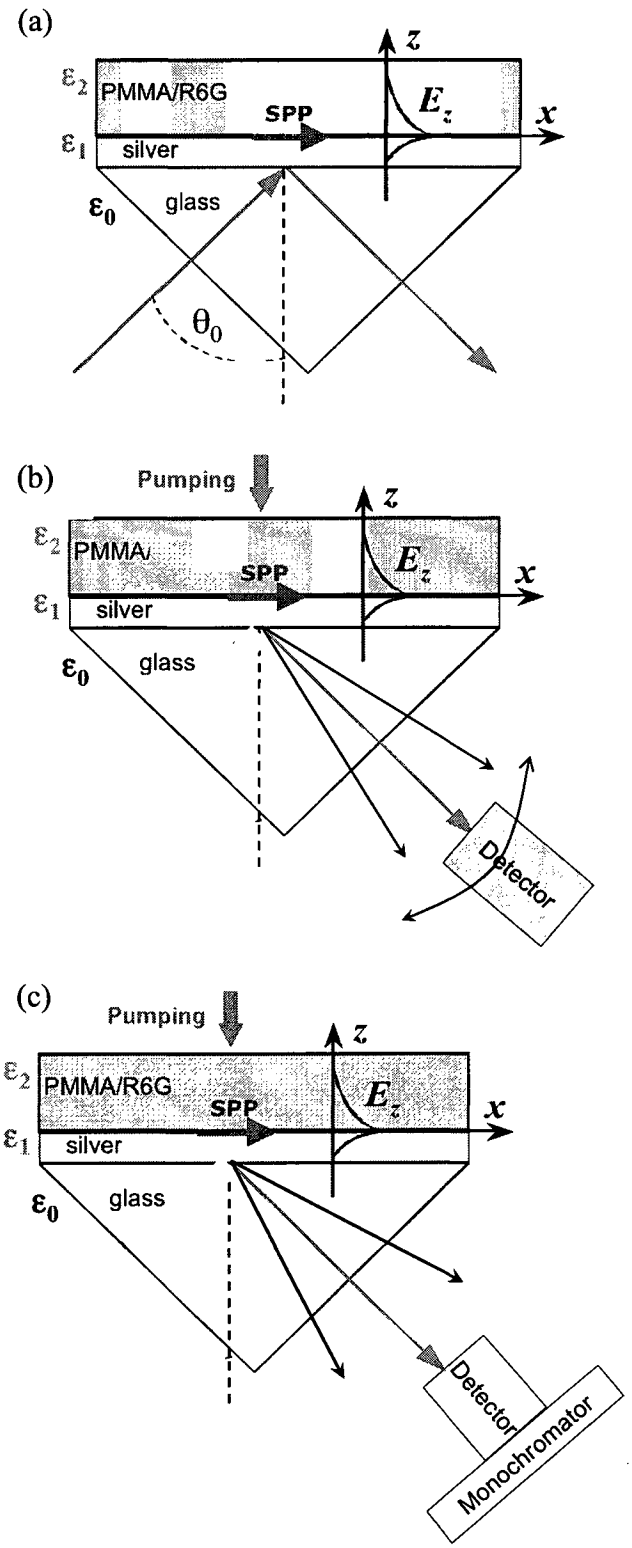

Figure 5.1 Experimental samples and setups: (a) used in exp.(1), (b) used in exp. (2), (c) used in exps. (3) and (4)

(2) Unintentional scatterers are always present in polymeric films and can even provide for a feedback in polymer random lasers [87]. In our system scatterers enable excitation of surface plasmon polaritons *via* coupling of incident light into SPP modes. Experimentally, SPPs were excited *via* pumping the PMMA film, and the intensity of light I decoupled to the prism was studied as a function of angle θ, as shown in Figure 5.1 (b).

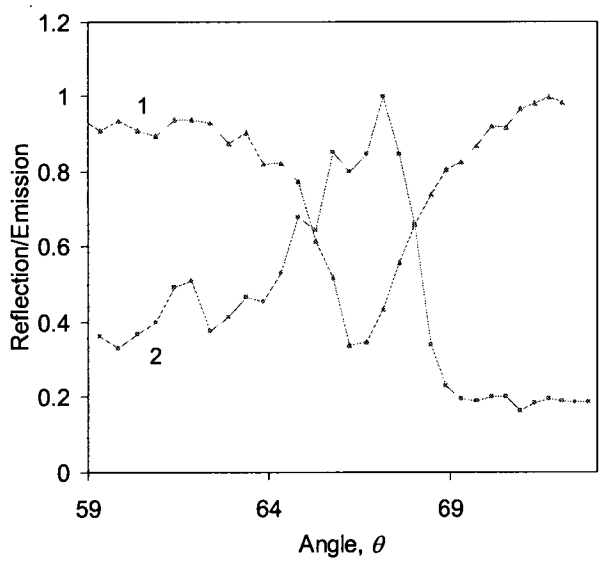

Figure 5.2 The angular profile of reflectivity (trace 1) with λ=575 nm; angular profile of emission originating from decoupling of scattering-induced SPPs (trace 2) measured from Exp. 2, Figure 5.2(b). The thickness of the silver in the sample is 62nm.

The angular profile of the decoupled light intensity $I(\theta)$ had a maximum almost at the same resonance angle θ_0, at which the reflectivity profile $R(\theta)$ had its minimum, Figure 5.2. This confirms that the detected light was, indeed, due to pumping-induced SPPs. The demonstrated effortless method of excitation of SPPs does not require any prism or grating and can be regarded as a "poor man's " technique.

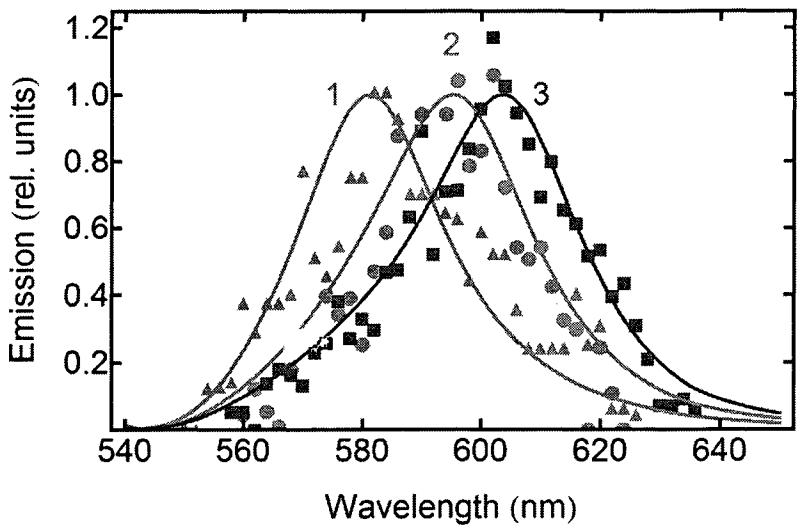

Figure 5.3 Spectra of SPP spontaneous emission decoupled at different angles θ; characters – experiment; solid lines – transfer matrix simulations; triangles and trace 1 – θ=67.17°, circles and trace 2 – θ=66.14°, squares and trace 3 – θ=65.62°. The thickness of the silver film is 57 nm.

(3) Alternatively, the SPPs can be excited *via* emission of R6G molecules, as shown in Figure 5.1 (c). The laser light at λ=532 nm corresponds to the absorption maximum of R6G. It excites dye molecules in the PMMA/R6G volume, in particular, in the vicinity of the silver film where the pumping-induced SPP is confined. Excited dye molecules, in turn, partly emit to SPP modes at corresponding frequencies. The SPPs excited by optically pumped molecules (reported earlier in Refs. [88, 89]) get decoupled to the prism at the angles corresponding to the SPPs' wavenumbers. At low pumping intensity, the SPP spectra recorded at different angles θ qualitatively resembled the R6G spontaneous emission spectrum modulated by the SPP decoupling function, Figure 5.3. Furthermore, the angular emission profiles $I(\theta)$ recorded at different wavelengths matched the

reflectivity profiles $R(\theta)$, Figure 5.4. This confirms that the observed emission was, in fact, due to decoupling of SPPs excited by pumped R6G molecules.

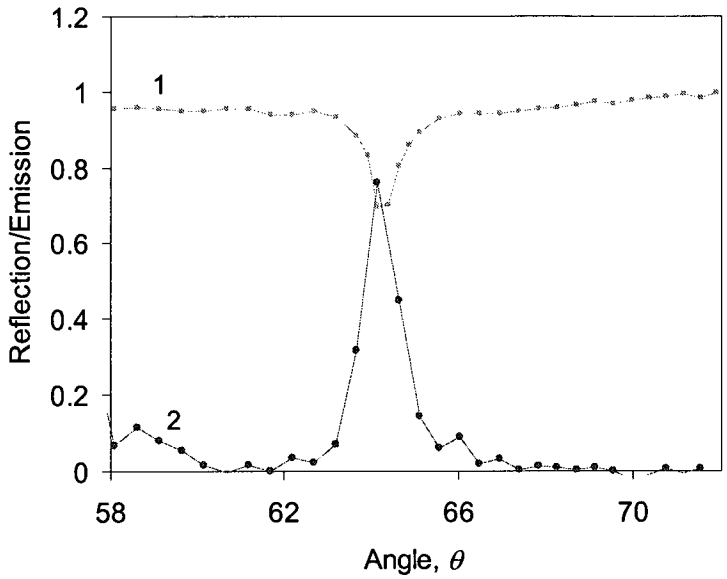

Figure 5.4 The angular profile of reflectivity (trace 1) with λ=632.8 nm. Angular profile of emission originating from decoupling of scattering-induced SPPs (trace 2) measured from Exp. 3, Figure 5.2(c). The thickness of silver in the sample is 81nm.

(4) The character of SPP emission excited *via* optically pumped dye molecules has changed dramatically at high pumping intensity.

(*i*) The emission spectra considerably narrowed in comparison to those at low pumping, Figure 5.5.

(*ii*) The narrowed emission spectra peaking at ~602 nm became almost independent of the observation angle.

(*iii*) The dependence of the emission intensity (recorded in the maximum of the emission spectrum) on the pumping intensity was strongly nonlinear with the distinct threshold, Figure 5.6.

(*iv*) The value of the threshold I_{th} depended on the observation angle θ. The angular dependence $I_{th}(\theta)$, resembled the angular profile of the reflectivity $R(\theta)$, Figure 5.7.

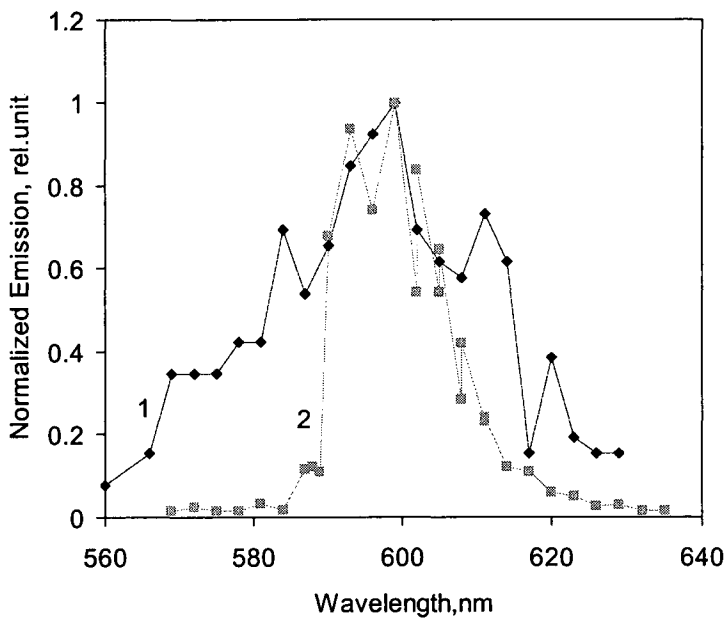

Figure 5.5 Spectra of the SPP emission recorded at θ=68.7° at low pumping density 10.9 mJ/cm^2 (diamonds) and high pumping density 81.9 mJ/cm^2 (squares). Trace 1 - below threshold; trace 2 – above threshold. The thickness of silver film is 39nm.

The experimental results above suggest the *stimulated* character of emission decoupled from SPP mode(s). To prove that the stimulated emission seen in our experiments comes from direct generation of SPPs rather than from random lasing in PMMA/R6G film, we studied the emission collected from the back side of the prism as

well as from glass slides with similar deposited films, close to the normal angle of incidence and at a grazing angle.

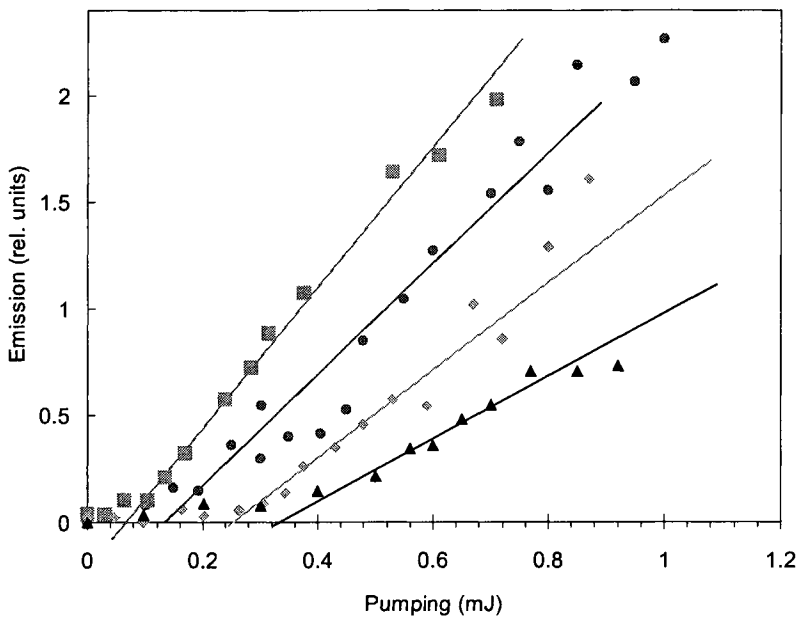

Figure 5.6 Input-output curves of SPP emission recorded at different angles θ. The thickness of the silver film is 39 nm. The diameter of the pumped spot is 2.16 mm, λ=602 nm. Squares – θ= 63.17°, circles – θ= 68.70°, diamonds – θ= 59.12°, triangles – θ= 70.35°. Resonance angle – θ_0 = 65.56°.

Experimentally, PMMA films doped with rhodamine 6G (R6G) dye in concentration 2.2×10^{-2}M were deposited on the glass slides. As shown in Figure 5.8, at high pumping energy, the collected emission from the above sample spectrally narrowed and demonstrated a threshold input-output behavior. However, the values of the thresholds (higher at nearly normal direction than at a grazing angle) were significantly larger than the threshold in the case of SPPs decoupled to the prism, and the narrowed

emission spectra of the glass slides covered with PMMA/Dye film had their maxima at wavelengths as short as ~584 nm, Figure 5.8 (inset).

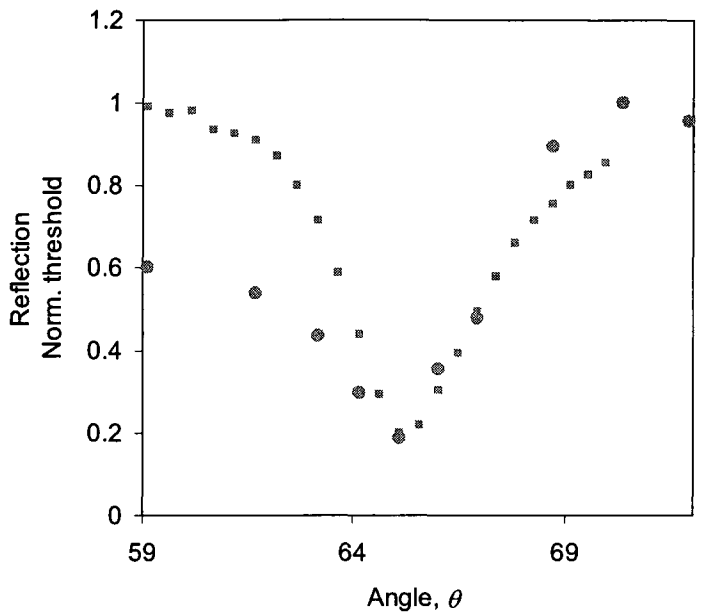

Figure 5.7 Dependence of the SPP stimulated emission threshold vs θ (circles) and the reflectivity profile (squares) measured at λ≈604 nm.

We thus conclude that the emission decoupled to the glass prism was generated by SPPs rather than originated in purely photonic modes within the PMMA/R6G layer above the silver film.

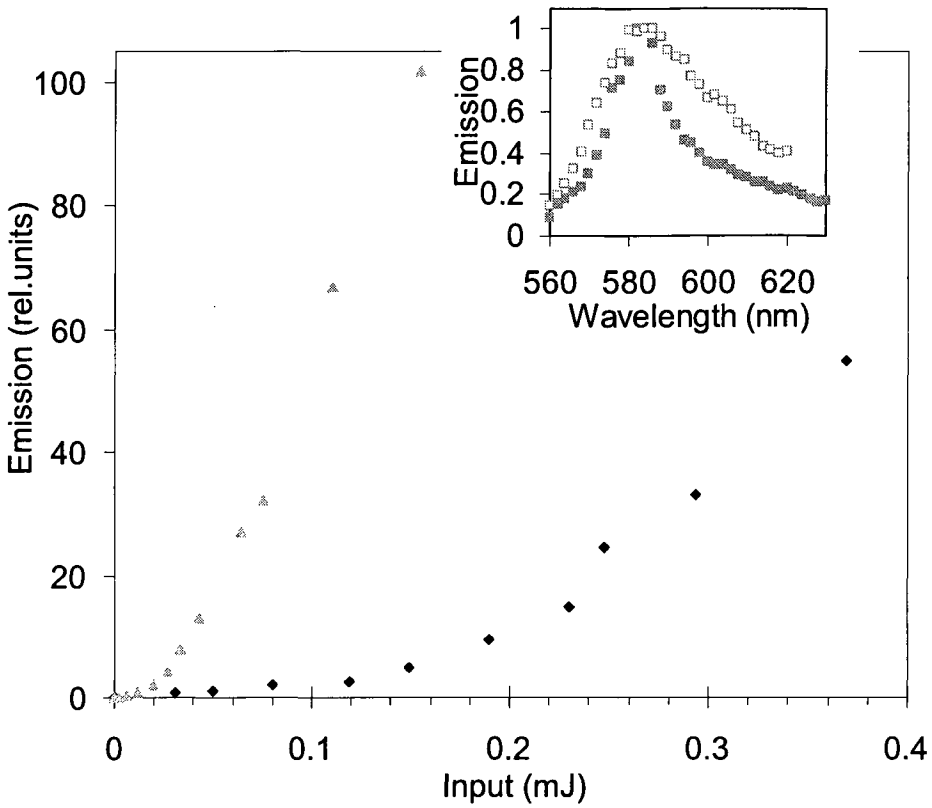

Figure 5.8 Input-output curves of SPP emission (triangles) and random laser emission (diamonds). The two measurements have the same spot size. Inset, spectra of the random laser emission from the glass slides coated with PMMA/Dye film recorded at low pumping energy 0.03 mJ (open squares) and high pumping energy 0.23 mJ (solid squares). In the measurement, the detector is at grazing angle to the sample.

5.3 Model Analysis

To further analyze the SPP emission observed in our experiments, we numerically solve Maxwell's equations with the transfer matrix approach [90]. In our simulations we first approximate the emitter by a point dipole and represent its field as a series of plane waves with well-defined x components of the wave vectors through Fourier expansion. We then solve for propagation of individual components of this expansion using the transfer-matrix method (TMM) [91]. The resulting set of solutions represents the set of

waveguide modes of open-waveguide structure formed by the finite-thickness metal film, the prism and the gain material [92]. Correspondingly, the total field resulting from the coupled to SPP emission is represented as a sum of these modes. This process allows us to directly calculate the field distribution in the system as well as to analyze angular and spectral distributions of the emitted signals below lasing threshold. The excellent agreement between experimental and theoretical SPP emission spectra at three different decoupling angles is shown in Figure 5.3. [90]

The TMM simulations [90], assuming linear behavior of the system in the frequency domain, are inapplicable above the lasing threshold. To qualitatively assess the onset of lasing oscillations, we use the following Fourier-transform-based approach. We first assume that SPP propagating in the x direction and decaying along its propagation is characterized by the complex wave vector $k_x=k_x'+k_x''j$, such that

$$E = E_0 e^{ik_x' x} e^{-k_x'' x} \tag{5.1}$$

where E is the SPP electric field and E_0 is its amplitude at x=0. The spectrum of this SPP in a wavenumber domain is given by the Fourier transform [90]

$$E(k) = \frac{1}{\pi}\int_0^{x'} E(x) e^{-ikx} dx = \frac{1}{\pi\left[-k_x'' + i\left(k_x' - k\right)\right]}, \tag{5.2}$$

where $x'=\infty$. Thus, similar to the case of TMM calculations described above, a single leaky SPP can be represented by a linear combination of open waveguide modes. Each of these modes is formed by the SPP coupled to two plane waves (incoming and outgoing) propagating at given angle θ in the prism. The relative contribution of each mode to total absorption/emission of the system, given by Eqn. (5.2), corresponds to Lorentzian

distribution of decoupled light intensity about the resonant value of the wave vector and, in particular, determines the shape of the dip in the reflectivity profile *R(θ)*, which is routinely recorded in SPP experiments in the attenuated total reflection geometry, Fig. 5.1 (a).

When gain in the system overcomes loss, the negative sign in the second exponent of Eqn. (5.1) changes to positive, which corresponds to exponential increase of the SPP intensity. In this case, if the upper limit of integration in Eqn. (5.2) is set to be equal to infinity, the integral diverges, which physically corresponds to the fact that no steady-state gain can exist (or be physically supported by any source of pumping) in an infinitely large system. However, if the upper limit of integration is set at a finite value (the condition, which simulates a pumped spot of a finite size) then the integral can be readily solved analytically. [90]

The Lorentzian-like spectrum of SPP emission $I_{SPP}(k) \propto |E(k)|^2$, calculated for SPP propagation with amplification, has a maximum at the resonance wavenumber k_x', Figure 5.9, in agreement with the experimentally observed reduction of the SPP lasing threshold at the resonant angle, Figure 5.8. When emission intensities $I_{SPP}(k)$ calculated at fixed wave vector $k_x^{'}$ and different values of gain $k_x^{''}$ (pumping energies) are plotted against $k_x^{''}$, the dependence, characterized by a distinct threshold, has a qualitative similarity with input-output curves measured experimentally, Figures 5.6 and 5.10.

The demonstrated phenomenon adds a new stimulated emission source to the toolbox of nanophotonic materials and devices and proves that total compensation by metamaterials' loss by gain is, indeed, possible.

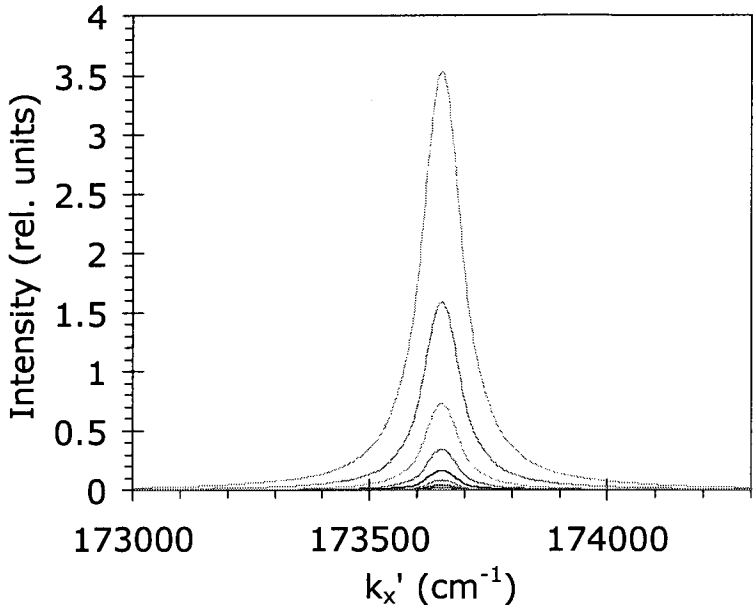

Figure 5.9 Calculated SPP spectra in the wavenumber domain. The values of gain in the SPP system (from high to low) correspond to k_x"=-50, -45, -10, -5, -1, 0 cm^{-1}. $\varepsilon_0 = n_0^2 = 3.18$, $\varepsilon_1 = -13.6 + 0.75j$, $\varepsilon_2 = 2.25$; $\lambda = 594.1$ nm). The thickness of the silver film is 39 nm. [90]

Knowing the concentration of R6G molecules in the film (1.3×10^{19} cm^{-3}), absorption and emission cross sections of R6G ($\sigma_{abs}^{\lambda=532nm} = 4.3 \times 10^{-16}$ cm^2, $\sigma_{em}^{\lambda=600nm} = 1.9 \times 10^{-16}$ cm^2), and lifetime of excited R6G molecules at given concentration of dye, τ=1 ns [83], we were able to evaluate the experimental threshold gains to be of the same order of magnitude as the theoretically predicted ones satisfying the condition $(\gamma_i + \gamma_r) = 0$. Thus, although nonlinear dependence of the SPP intensity on the pumping intensity and narrowing of the emission spectrum are expected even below the threshold, a good agreement between the theoretical and the experimental results serves as a strong indication that the observed emission is due to stimulated emission of SPPs in a regime when the total gain in the system exceeds the total loss [90].

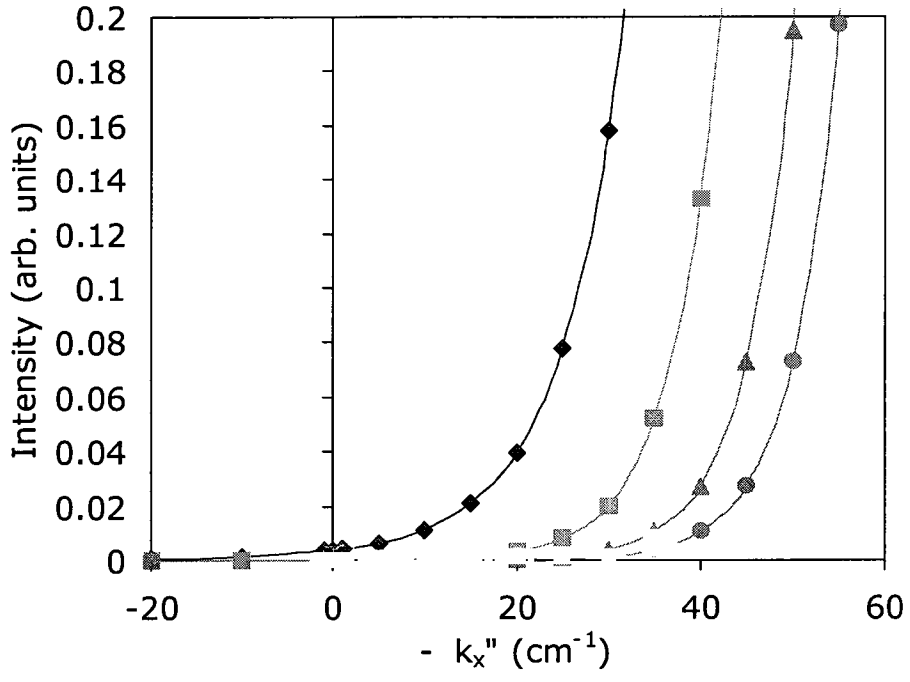

Figure 5.10 Input-output curves of SPP emission calculated above the threshold at $k_x' = 173{,}660\ cm^{-1}$ (close to the resonance) – diamonds, $173{,}740\ cm^{-1}$ – squares, $173{,}860\ cm^{-1}$ – triangles, and $174{,}000\ cm^{-1}$ – circles.[90]

5.4 Discussion and Summary

To summarize, we have studied surface plasmon polaritons (SPPs) excited by emission of optically pumped rhodamine 6G (R6G) molecules and by direct scattering of pumping light in a polymeric film in the attenuated total reflection setup. We have observed laser-like emission of SPPs decoupled to the glass prism. In particular, the input-output dependence had a distinctive threshold and the emission spectrum narrowed considerably above the threshold. The threshold and the overall emission intensity strongly depended on the SPP decoupling angle. Thus, the threshold was minimal and the

emission intensity was maximal at the resonance condition, at which the wave vector of the SPP k_{SPP} was equal to the projection of the photon wave vector to the metal-dielectric interface k_x^{phot}. This behavior is in a good agreement with the model considering SPP propagation with amplification, when the total gain in the system exceeds the total loss. Random laser effect, which occurred in R6G doped polymeric film at high pumping, had a different spectrum and a different threshold than the SPP emission. That is why we ruled it out as a possible source of the laser-like SPP behavior. The experimental thresholds of SPP stimulated emission had the same order of magnitude as the theoretically predicted ones. The observed phenomenon may be relevant to SPASER proposed in Ref. [62]. However, the existence of the stimulated emission feedback, which is a key element of SPASER, was not confirmed in our system. Moreover, in contrast to SPASER that generates localized SPs, our system generates propagating SPP waves.

Note that unintentional scatterers, which are common to polymeric films, provide for stimulated emission feedback in many polymer random lasers [87]. The same scattering centers plus scatterers associated with the metallic film can potentially provide for feedback of the SPP stimulated emission. Although this feedback is possible and even likely, we do not have experimental evidence of its existence.

Chapter 6

SUMMARY

Many applications of nanoplasmonic materials and devices are hindered by the strong absorption loss in metal. In this dissertation, we have developed several techniques allowing to significantly reduce the loss. In particular:

(1) We have demonstrated the suppression of loss of surface plasmon polariton propagating at the interface between silver film and optically pumped polymer with dye. We have experimentally achieved the optical gain in the dielectric (PMMA film with R6G dye) equal to 420 cm-1. In the case of thick low-loss silver film and low index dielectric, the demonstrated value of gain is sufficient for compensation of the total loss hindering the propagation of surface plasmon polariton. The large magnitude of the effect enables a variety of applications of "active" nanoplasmonics.

(2) We have observed laser-like emission of surface plasmon polaritons (SPPs) decoupled to the glass prism in an attenuated total reflection setup. SPPs were excited by optically pumped molecules in a polymeric film deposited on the top of the silver film. Stimulated emission was characterized by a distinct threshold in the input-output dependence and narrowing of the emission spectrum. The observed stimulated emission, and corresponding to it, compensation of the metallic absorption loss by gain enables many applications of metamaterials and nanoplasmonic devices.

(3) We have demonstrated that an addition of highly concentrated rhodamine 6G chloride dye to the PMMA film adjacent to a silver film can cause 30% elongation of the propagation length of surface plasmon polaritons (SPPs). The possibility to elongate the SPP propagation length without optical gain opens a new technological dimension to low-loss nanoplasmonic and metamaterials.

REFERENCES

1. R. H. Ritchie, "Plasma losses by fast electrons in thin film," *Phys. Rev.* 106, pp. 874-881, 1957.
2. C. J. Powell and J. B. Swan, "Origin of characteristic electron energy losses in Aluminum," *Phys. Rev.* 115, pp. 869-875, 1959.
3. C. J. Powell and J. B. Swan, "Origin of characteristic electron energy losses in Magnesium," *Phys. Rev.* 116, pp. 81-83, 1959.
4. E. A. Stern and R. A. Ferrell, "Surface plasma oscillations of a degenerate electron gas," *Phys. Rev.* 120, pp. 130-136, 1960.
5. D. L. Jeanmaire and P. Richard, Surface Raman Electrochemistry Part I. Heterocyclic, "Aromatic and aliphatic amines adsorbed on the anodized silver electrode," *J. Electroanal. Chem.* 84, pp. 1–20, 1977.
6. J. B. Pendry, "Negative refraction makes a perfect lens," *Phys. Rev. Lett.* 85, pp. 3966-3969, 2000.
7. Z. Jacob, L. V. Alekseyev, and E. Narimanov, "Optical Hyperlens: Far-field imaging beyond the diffraction limit," *Opt. Express* 14, pp. 8247-8256, 2006.
8. A. Salandrino and N. Engheta, "Far-field subdiffraction optical microscopy using metamaterial crystals: Theory and simulations," *Phys. Rev. B* 74, 075103 (7 pages), 2006.
9. Z. Liu, H. Lee, Y. Xiong, C. Sun, and X. Zhang, "Far-field optical hyperlens magnifying sub-diffraction-limited objects," *Science* 315, pp. 1686-1686, 2007.

10. I. I. Smolyaninov, Y. –J. Hung and C. C. Davis, "Magnifying superlens in the visible frequency range," *Science* 315, pp. 1699-1701, 2007.

11. D. Schurig, J. J. Mock, B. J. Justice, S. A. Cummer, J. B. Pendry, A. F. Starr, and D. R. Smith, "Metamaterial Electromagnetic Cloak at Microwave Frequencies," *Science* 314, pp. 977-980, 2006.

12. W. Cai, U. K. Chettiar, A. V. Kildishev, and V. M. Shalaev, "Optical cloaking with metamaterials," *Nature Photonics* 1, pp. 224-227, 2007.

13. P. Mühlschlegel, H. -J. Eisler, O. J. F. Martin, B. Hecht, and D. W. Pohl, "Resonant optical antennas," *Science* 308, pp. 1607-1609, 2005.

14. J. A. Gordon and R. W. Ziolkowski, "The design and simulated performance of a coated nano-particle laser," *Opt. Express* 15, pp. 2622-2653, 2007.

15. S. Noda, "Applied physics: Seeking the Ultimate Nanolaser," *Science* 314, pp. 260-261, 2006.

16. R. H. Ritchie, "Surface plasmons in solids," *Surf. Sci.* 34, 1, pp. 1-19, 1973.

17. M. Fleischmann, P. J. Hendra, and A. J. McQuillan, "Raman spectra of pyridine adsorbed at a silver electrode," *Chem. Phys. Lett.* 26, pp. 163-166, 1974.

18. M. Moskovits, "Surface-enhanced spectroscopy," *Rev. Mod. Phys.* 57, pp. 783-826, 1985.

19. M. Quinten, A. Leitner, J. R. Krenn, and F. R. Aussenegg, "Electromagnetic energytransport via linear chains of silver nanoparticles," *Opt. Lett.* 23, pp. 1331-1333, 1998.

20. R. D. Averitt, S. L. Westcott, and N. J. Halas, "Linear optical properties of gold nanoshells," *J. Opt. Soc. Am. B* 16, pp. 1824-1832, 1999.

21. M. L. Brongersma, J. W. Hartman, and H. A. Atwater, "Electromagnetic energy transfer and switching in nanoparticle chain arrays below the diffraction limit," *Phys. Rev. B* 62, R16356 (3 pages), 2000.

22. T. Pham, J. B. Jackson, N. J. Halas, and T. R. Lee, "Preparation and Characterization of Gold Nanoshells Coated with Self-Assembled Monolayers," *Langmuir* 18, pp. 4915-4920, 2002.

23. J. J. Mock, M. Barbic, D. R. Smith, D. A. Schultz, and S. Schultz, "Shape effects in Plasmon resonance of individual colloidal silver nanoparticles," *Chem. Phys.* 116, pp. 6755-6759, 2002.

24. U. Kreibig and M. Vollmer, *Optical Properties of Metal Clusters*, Springer, New York, vol. 25, 1995

25. K.-H. Su, Q.-H. Wei, X. Zhang, J. J. Mock, D. R. Smith, and S. Schultz, "Interparticle coupling effects on plasmon resonances of nanogold particles," *Nano Let.* 3, pp. 1087- 1090, 2003.

26. M. Quinten, "Optical effects associated with aggregates of clusters," *J. Cluster Sci.* 10, pp. 319-358, 1999.

27. K. Kneipp, Y. Wang, H. Kneipp, L. T. Perelman, I. Itzkan, R. R. Dasari, and M. S. Feld, "Single molecule detection using surface-enhanced Raman scattering (SERS)," *Phys. Rev. Lett.* 78, pp. 1667–1670, 1997.

28. S. Nie and S. R. Emory, "Probing single molecules and single nanoparticles by surfaceenhanced Raman scattering," *Science* 275, pp. 1102–1104, 1997.

29. L. E. Brus and A. Nitzan, "Chemical processing using electromagnetic field enhancement," U.S. Patent No.: 4,481,091 (21 October, 1983), Chemical processing using electromagnetic field enhancement.

30. L. Hutson, "Golden Eye," *Mater. World* 13, No. 6, 2005.

31. D. M. Schaadt, B. Feng, and E. T. Yu, "Enhanced semiconductor optical absorption via surface plasmon excitation in metal nanoparticles," *Appl. Phys. Lett.* 86, 063106 (3 pages), 2005.

32. T. L. Ferrell, "Thin-foil surface-plasmon modification in scanning-probe microscopy," *Phys. Rev. B* 50, pp 14738-14741, 1994.

33. E. J. Sanchez, L. Novotny, and X. S. Xie, "Near-field fluorescence microscopy based on two-photon excitation with metal tips," *Phys. Rev. Lett.* 82, pp. 4014–4017, 1999.

34. M. I. Stockman, "Possibility of laser nanomodification of surfaces with the use of the scanning tunneling microscope," *Optoelectr., Instrum. Data Process.* 3, pp. 27–37, 1989.

35. H. F. Ghaemi, T. Thio, D. E. Grupp, T. W. Ebbesen, and H. J. Lezec, "Surface plasmons enhance optical transmission through subwavelength holes," *Phys. Rev. B* 58, 6779-6782, 1998.

36. N. Bonod, R. Reinisch, E. Popov, and M. Neviere, "Optimization of surface-plasmonenhanced magneto-optical effects," *J. Opt. Soc. Am. B* 21, pp. 791-797, 2004.

37. V. G. Veselago, "The electrodynamics of substances with simultaneously negative values of ε and μ," *Soviet Physics Uspekhi* 10, no. 4, pp. 509-514, 1968.

38. D. R. Smith, Willie J. Padilla, D. C. Vier, S. C. Nemat-Nasser, and S. Schultz, "Composite Medium with Simultaneously Negative Permeability and Permittivity," *Phys. Rev. Lett.* 84, pp. 4184–4187, 2000.

39. R. A. Shelby, D. R. Smith, and S. Schultz, "Experimental Verification of a Negative Index of Refraction," *Science* 292, pp.77-79, 2001.

40. N. Fang, H. Lee, and X. Zhang, "Sub-diffraction-limited optical imaging with a silver superlens," *Science* 308, pp. 534-537, 2005.

41. D. O. S. Melville and R J. Blaikie, "Super-resolution imaging through a planar silver layer," *Opt. Express* 13, pp. 2127-2134, 2005.

42. T. J. Yen, W. J. Padilla, N. Fang, D. C. Vier, D. R. Smith, J. B. Pendry, D. N. Basov, and X. Zhang, "Terahertz magnetic response from artificial materials," *Science* 303, pp.1494-1496, 2004.

43. S. Linden, C. Enkrich, M. Wegener, J. Zhou, T. Koschny, and C. M. Soukoulis, "Magnetic response of metamaterials at 100 terahertz," *Science* 306, pp. 1351- 1353, 2004.

44. S. Zhang, W. Fan, B. K. Minhas, A. Frauenglass, K. J. Malloy, and S. R. J. Brueck, "Midinfrared resonant magnetic nanostructures exhibiting a negative permeability", *Phys. Rev. Lett.* 94, pp. 037402/1-4, 2005.

45. V. A. Podolskiy, A. K. Sarychev, and V. M. Shalaev, "Plasmon modes in metal nanowires and left-handed materials," *J. of Nonlinear Opt. Phys. and Mat.* 11, pp. 65-74, 2002.

46. V. A. Podolskiy, A. K. Sarychev, and V. M. Shalaev, "Plasmon modes and negative refraction in metal nanowire composites," *Opt. Express* 11, pp. 735-745, 2003.

47. V. A. Podolskiy, A. K. Sarychev, E. E. Narimanov, and V. M. Shalaev "Resonant light interaction with plasmonic nanowire systems," *J. Opt. A: Pure Appl. Opt.* 7, pp. S32–S37, 2005.

48. V. M. Shalaev, W. Cai, U. Chettiar, H.-K. Yuan, A. K. Sarychev, V. P. Drachev, and A. V. Kildishev, "Negative Index of Refraction in Optical Metamaterials," *Opt. Lett.* 30, pp. 3356- 3358, 2005; arXiv:physics/0504091, Apr. 13, 2005.

49. A. V. Kildishev, W. Cai, U. Chettiar, H.-K. Yuan, A. K. Sarychev, V. P. Drachev, and V. M. Shalaev, "Negative Refractive Index in Optics of Metal-Dielectric Composites," *J. Opt. Soc. Am. B* 23(3), pp. 423-433, 2006.

50. V. P. Drachev, W. Cai, U. Chettiar, H.-K. Yuan, A. K. Sarychev, A. V. Kildishev, and V. M. Shalaev, "Experimental verification of optical negative-index materials," Laser *Phys. Lett.* 3, pp. 49-55 (2006) / DOI 10.1002/lapl.200510062.

51. U. K. Chettiar, S. Xiao, A. V. Kildishev, W. Cai, H. Yuan, V. P. Drachev, and Vladimir M. Shalaev, "Optical Metamagnetism and Negative-Index Metamaterials," *MRS BULLETIN*, 33, pp. 921-926, 2008.

52. A. N. Sudarkin and P. A. Demkovich, "Excitation of surface electromagnetic waves on the boundary of a metal with an amplifying medium," *Sov. Phys. Tech. Phys.* 34, pp. 764-766, 1989.

53. B. Ya. Kogan, V. M. Volkov, and S. A. Lebedev, "Superluminescence and generation of stimulated radiation under internal-reflection conditions," *JETP Lett.* 16, pp. 100-105, 1972.

54. G. A. Plotz, H. J. Simon, and J. M. Tucciarone, "Enhanced total reflection with surface plasmons," *J. Opt. Soc. Am. A* 69, pp. 419-421, 1979.

55. M. P. Nezhad, K. Tetz, and Y. Fainman, "Gain assisted propagation of surface plasmon polaritons on planar metallic waveguides," *Opt. Express* 12, pp. 4072-4079, 2004.

56. I. Avrutsky, "Surface plasmons at nanoscale relief gratings between a metal and a dielectric medium with optical gain," *Phys. Rev. B 70*, 155416 (6 pages), 2004.

57. J. Seidel, S. Grafstroem, and L. Eng, "Stimulated emission of surface plasmons at the interface between a silver film and an optically pumped dye solution," *Phys. Rev. Lett.* 94, pp.177401 (4 pages), 2005.

58. N. M. Lawandy, "Localized surface plasmon singularities in amplifying media," *Appl. Phys. Lett.* 85, pp. 540-542, 2004.

59. H. C. van de Hulst, *Light Scattering by Small Particles*, Dover, New York, 1981.

60. M. A. Noginov, G. Zhu, M. Bahoura, J. Adegoke, C. E. Small, B. A. Ritzo, V. P. Drachev, and V. M. Shalaev, "Enhancement of surface plasmons in an Ag aggregate by optical gain in a dielectric medium," *Opt. Lett.* 31, pp. 3022-3024, 2006.

61. N. M. Lawandy, "Nano-particle plasmonics in active media," in *Proceedings of SPIE Vol. 5924, Complex mediums VI: Light and Complexity*, edited by M. W. McCall, G. Dewar, and M. A. Noginov, (SPIE, Bellingham, WA, 2005) pp. 59240G/1-13, 2005.

62. D. J. Bergman and M. I. Stockman, "Surface plasmon amplification by stimulated emission of radiation: Quantum generation of coherent surface plasmons in nanosystems," *Phys. Rev. Lett.* 90, pp. 027402/1–4, 2003.

63. M. I. Stockman, "Ultrafast, nonlinear, and active nanoplasmonics," in *Proceedings of SPIE Vol. 5924, Complex mediums VI: Light and Complexity*, edited by M. W.

McCall, G. Dewar, and M. A. Noginov, (SPIE, Bellingham, WA, 2005) pp. 59240F/1-12, 2005.

64. H. Raether, *Surface plasmons on smooth and rough surfaces and on gratings*, Springer-Verlag, Berlin, 1988.

65. Y. Teng and E. A. Stern, "Plasma radiation from metal grating surfaces," *Phys. Rev. Lett.* 19, pp. 511-514, 1967.

66. A. Otto, "Excitation of non-radiative surface plasma waves in silver by the method of frustrated total reflection," *Z. Phys.* 216, pp. 398-410, 1968.

67. E. Kretschmann, "Determination of the optical constants of metals by excitation of surface plasmons," *Z. Phys.* 241, pp. 313-324, 1971.

68. M. A. Noginov, V. A. Podolskiy, G. Zhu, M. Mayy, M. Bahoura, J. A. Adegoke, B. A. Ritzo, and K. Reynolds, "Compensation of loss in propagating surface plasmon polariton by gain in adjacent dielectric medium," *Opt. Express* 16, pp.1385-1392, 2008.

69. H. Shin and S. Fan, "All-angle negative refraction for surface plasmon waves using a metal-dielectric-metal structure," *Phys. Rev. Lett.* 96, pp. 073907, 2006.

70. G. Dolling, C. Enkrich, M. Wegener, C. M. Soukoulis, and S. Linden, "Simultaneous negative phase and group velocity of light in a metamaterial," *Science* 312, pp. 892-894, 2006.

71. A. Alu and N. Engheta, "Optical nanotransmission lines: synthesis of planar left-handed metamaterials in the infrared and visible regimes," *J. Opt. Soc. Am. B* 23, pp. 571-583, 2006.

72. Y. Chen, P. Fisher, and F. W. Wise, "Negative refraction at optical frequencies in nonmagnetic two-component molecular media," *Phys. Rev. Lett.* 95, pp. 067402, 2005.

73. T. Mackay and A. Lakhtakia, "Comment on 'negative refraction at optical frequencies in nonmagnetic two-component molecular media'," *Phys. Rev. Lett.* 96 pp. 159701, 2006.

74. Y. Chen, P. Fisher, and F. W. Wise, "Chen, Fischer, and Wise Reply:," *Phys. Rev. Lett.* 96 pp.159702, 2006.

75. P. B. Johnson and R. W. Christy, "Optical Constants of the Noble Metals," *Phys. Rev. B* **6**, pp.4370-4379, 1972.

76. M. V. Klein and T. E. Furtak, *Optics*, 2nd ed., Wiley, New York, 1986.

77. G. Zhu, M. Mayy, M. Bahoura, B. A. Ritzo, H. V. Gavrilenko, V. I. Gavrilenko, and M. A. Noginov , "Elongation of surface plasmon polariton propagation length without gain," *Opt. Express* 16, pp. 15576-15583, 2008.

78. H. Ehrenreich and H. R. Phillip, "Optical properties of Ag and Cu," *Phys. Rev.* 128, pp.1622-1629, 1962.

79. J. H. Simmons and K. S. Potter, *Optical Materials*, Academic Press, San Diego, 2000.

80. K. Stahrenberg, T. Herrmann, N. Esser, J. Sahm, W. Richter, S. V. Hoffmann, and Ph. Hofmann. "Surface state contrubution of the optical anisotropy of Ag(110) surface: a reflectance anisotropy spectroscopy and photoemission study," *Phys. Rev. B* 58, R10207, 1998.

81. D. W. Lynch and W. R. Hunter, "Comments on the optical constants of metals and an introduction to data for several metals," in *Handbook of optical constants of solids, Part II*, ed. by E. D. Palik, Academic Press, NY, 1985.

82. A. A. Govyadinov and V. A. Podolskiy, "Gain-assisted slow to superluminal group velocity manipulation in nano-waveguides," *Phys. Rev. Lett.* 97, 223902, 2006.

83. K. Selanger, A. J. Falnes, and T. Sikkeland, "Fluorescence lifetime studies of Rhodamine 6G in methanol," *J. Phys. Chem.* 81, pp. 1960-1963, 1977.

84. C. Sirtori, C. Gmachl, F. Capasso, J. Faist, D. L. Sivco, A. L. Hutchinson, and A. Y. Cho, "Long-wavelength ($\lambda \approx 8$–11.5 μm) semiconductor lasers with waveguides based on surface plasmons," *Opt. Lett.* 23, pp. 1366-1368, 1998.

85. A. Tredicucci, C. Gmachl, F. Capasso, A. L. Hutchinson, D. L. Sivco, and A. Y. Cho, "Single-mode surface-plasmon laser," *Appl. Phys. Lett.* 76, pp. 2164-2166, 2000.

86. Y. Ling, H. Cao, A. L. Burin, M. A. Ratner, X. Liu, and R. P. H. Chang, "Investigation of random lasers with resonant feedback," *Phys. Rev. A* 64, 063808 (8 pages), 2001.

87. M. A. Noginov, *Solid-State Random Lasers*, Springer, printed in the USA, 2005.

88. W. H. Weber and C. F. Eagen, "Energy transfer from an excited dye molecule to the surface plasmons of an adjacent metal," *Opt. Lett.* 4, pp. 236-238, 1979.

89. K. Ray, H. Szmacinski, J. Enderlein, and J. R. Lakowicz, "Distance dependence of surface plasmon-coupled emission observed using Langmuir-Blodgett films," *Appl. Phys. Lett.* 90, pp. 251116/1-3, 2007.

90. M. A. Noginov, G. Zhu, M. Mayy, B. A. Ritzo, N. Noginova, and V. A. Podolskiy, "Stimulated emission of surface plasmon polaritons", *Phys. Rev. Lett.* 101, 226806 (4 pages), 2008.

91. I. Avrutsky, "Guided modes in a uniaxial multiplayer," *J Opt. Soc. Am. A* 20, pp. 548-556, 2003.

92. V. V. Schevchenko, *Continuous Transitions in Open Waveguides*, Golem, Boulder, CO, 1971.

VITA

GUOHUA ZHU

Department of Electrical and Computer Engineering
Old Dominion University
Norfolk, Virginia, 23508
Office Phone: 757-823-9531
E-mail address: gzhux001@odu.edu; gzhu@nsu.edu

Education

Ph.D., Electrical and Computer Engineering, Aug. 2009 (Expected), Old Dominion University, Norfolk, Virginia

M.S. in Material Science, May 2002, Norfolk State University, Norfolk, Virginia

M.S. in Material Processing, March 1999, Shanghai Jiaotong Univerisity, P. R. China

B. S. in Materials Engineering, July 1994, Shanghai Jiaotong Univerisity, P. R. China

Publications

Book Chapters

1. M. A. Noginov, G. Zhu, and V. I. Gavrilenko, "Nonlinear emission of Au nanoparticles enhanced by rhodamine 6G dye," in *Nonlinear Optics and Applications*, Hossin A. Abdeldaem and Donald O. Frazier, eds., pp. 233-256, Research Signpost, Kerala, India, 2008.
2. M. A. Noginov, G. Zhu, V. M. Shalaev, and V. P. Drachev, "Surface plasmons and gain media," in *Advances in Nano-Optics and Nano-Photonics, Volume 2: Nano-Plasmonics*, editors: S. Kawata, V. M. Shalaev, Elsevier Science, ISBN: 978-0-444-52838-4, 2006.

Peer-reviewed Papers

1. M. A. Noginov, G. Zhu, A. M. Belgrave, R. Bakker, V. M. Shalaev, E. E. Narimanov, S. Stout, E. Herz, T. Suteewong, and U. Wiesner, "Demonstration of a 'spaser'-based nanolaser", published online by *Nature*, 16 August 2009
2. M. Mayy, G. Zhu, Yu. A. Barnakov, and M. A. Noginov, "Development of composite silver-polymer metamaterials," *J. Appl. Phys.* 105, 084318, 2009.
3. G. Zhu, M. Mayy, M. Bahoura, B. A. Ritzo, H. V. Gavrilenko, V. I. Gavrilenko, and M. A. Noginov, "Elongation of surface plasmon polariton propagation length without gain," *Opt. Express* 16, pp. 15576-15583, 2008.
4. G. Zhu, C. E. Small, and M. A. Noginov, "Single- and two-photon excitation of a GaAs random laser," *Opt. Lett.* 33, pp. 920-922, 2008.
5. M. A. Noginov, G. Zhu, M. Mayy, B. A. Ritzo, N. Noginova, and V. A. Podolskiy, "Stimulated Emission of Surface Plasmon Polaritons," *Phys. Rev. Lett.* 101, 226806 (4 pages), 2008.
6. N. Noginova, G. Zhu, M. Mayy, and M. A. Noginov, "Magnetic dipole based systems for probing optical magnetism," *J Appl. Phys.* 103, 07E901 (1-3), 2008.
7. M. A. Noginov, V. A. Podolskiy, G. Zhu, M. Mayy, M. Bahoura, J. A. Adegoke, B. A. Ritzo, and K. Reynolds, "Compensation of loss in propagating surface plasmon polariton by gain in adjacent dielectric medium," *Opt. Express* 16, pp. 1385-1392, 2008.
8. G. Zhu, V. I. Gavrilenko, M. A. Noginov, "Emission of Au nanoparticles with and without rhodamine 6G dye," *J. Chem. Phys.* 127, 104503/1-8, 2007.
9. G. Zhu, C. E. Small, and M. A. Noginov, "Control of gain and amplification in random lasers," *J Opt. Soc. Am. B* 24, pp. 2129-2135, 2007.
10. G. Zhu, M. Bahoura, M. A. Noginov, V. Vasilyev, K. P. Zhuravlev, and V. F. Zolin, "Vibronic and Raman spectra of $Y(Eu^{3+})$ polytantalate, $Eu_xY_{1-x}Ta_7O_{19}$," *Laser Physics* 17, pp. 818-823, 2007.
11. M. A. Noginov, G. Zhu, and V. I. Gavrilenko "Sensitized nonlinear emission of gold nanoparticles," *Opt. Express* 15, pp. 15648-15655, 2007.

12. M. A. Noginov, G. Zhu, M. Bahoura, J. Adegoke, C. Small, B. A. Ritzo, V. P. Drachev, and V. M. Shalaev, "The effect of gain and absorption on surface plasmons in metal nanoparticles," *Appl. Phys. B* 86(3), pp. 455-460, 2007.
13. M. A. Noginov, G. Zhu, M. Bahoura, J. Adegoke, C. E. Small, B. A. Ritzo, V. P. Drachev, and V. M. Shalaev, "Enhancement of surface plasmons in an Ag aggregate by optical gain in a dielectric medium", *Opt. Lett.* 31, pp. 3022-3024, 2006.
14. M. A. Noginov, G. Zhu, M. Bahoura, C. E. Small, C. Davison, and J. Adegoke, V. P. Drachev, P. Nyga, and V. M. Shalaev, "Enhancement of spontaneous and stimulated emission of a rhodamine 6G dye by an Ag aggregate," *Phys. Rev. B* 74, 184203/1-8 (2006).
15. M. A. Noginov, G. Zhu, C. Small, and J. Novak, "Neodymium random laser with external mirrors," *Appl. Phys. B: Lasers and Optics* 84, pp. 269 – 273 (2006).
16. M. A. Noginov, G. Zhu, C. Davison, A. K. Pradhan, K. Zhang, M. Bahoura, M. Codrington, V. P. Drachev, V. M. Shalaev, and V. F. Zolin, "Effect of Ag aggregate on spectroscopic properties of Eu:Y2O3 nanoparticles," *J. of Mod. Optics* 52, pp. 2331-2341, 2005.
17. M. A. Noginov, J. Novak, D. Grigsby, G. Zhu, and M. Bahoura, "Optimization of the transport mean free path and the absorption length in random lasers with non-resonant feedback," *Opt. Express* 13, pp. 8829-8836, 2005.
18. M. A. Noginov, I. N. Fowlkes, and G. Zhu, "Fiber-coupled random laser," *Appl. Phys. Lett.* 86, 161105 (3 pages), 2005.
19. M. Bahoura, K. J. Morris, G. Zhu, and M. A. Noginov, "Dependence of the Neodymium Random Laser Threshold on the Diameter of the Pumped Spot," *IEEE J. Quantum Electronics* 41, no. 5, pp. 677-685,2005.
20. M. A. Noginov, G. Zhu, I. Fowlkes, M. Bahoura, "GaAs random laser," *Laser Physics Lett.* 1, pp. 291-293, 2004.
21. M. A. Noginov, G. Zhu, A. A. Frantz, J. Novak, S. N. Williams, and I. Fowlkes, "Dependence of $NdSc_3(BO_3)_4$ random laser parameters on particle size," *J Opt. Soc. Am. B* 21, pp. 191-200, 2004.

22. M. A. Noginov, I. N. Fowlkes, G. Zhu, and J. Novak, "Random laser thresholds in cw and pulsed regimes," *Phys. Rev. A* 70, 043811(5 pages), 2004.